NOCTURNAL RELATIVE HUMIDITY MAXIMA ABOVE THE BOUNDARY LAYER IN THE AMERICAN MIDWEST: A DIAGNOSTIC FOR THE MOUNTAIN-PLAINS SOLENOIDAL CIRCULATION

by

Amanda Mercer

Submitted in partial fulfillment of the requirements
for the degree of Master of Science

at

Dalhousie University
Halifax, Nova Scotia
August 2017

Table of Contents

List of Figures . . . . . **iv**

Abstract . . . . . **vii**

List of Abbreviations and Symbols Used . . . . . **viii**

Acknowledgements . . . . . **xi**

Chapter 1 Introduction **1**

1.1 The Planetary Boundary Layer 1

1.1.1 Observing the depth of the PBL 1

1.1.2 Diurnal and Seasonal Cycles of PBL Depth 2

1.1.3 Boundary Layer Relative Humidity 3

1.1.4 Nocturnal Low Level Jet 4

1.2 Climatological features of interest in the American Midwest 6

1.2.1 Diurnal Cycle of Rainfall 6

1.2.2 The Mountain-Plains Solenoid 7

1.3 Atmospheric Tides and Surface Pressure Perturbations 8

Chapter 2 Nocturnal Relative Humidity Maxima above the Boundary Layer in the American Midwest: A Diagnostic for the Mountain-Plains Solenoidal Circulation **9**

2.1 Abstract 9

2.2 Motivation 10

2.3 Data Sets 12

2.3.1 Meteorological data from commercial aircraft 12

2.3.2 Vertical Motion from MERRA-2 Reanalysis 14

2.4 Nocturnal relative humidity maxima above the boundary layer 15

2.5 Interannual variability in lower tropospheric relative humidity 21

2.6 MERRA-2 vertical motion and relative humidity 25
2.7 Nocturnal LLJ 34
2.8 Conclusion 36
2.9 Acknowledgments 38
Chapter 3 Conclusion and Future Work **39**
References **42**
Appendix A: A.1 Copyright Information **47**

List of Figures

2.1 Map of midwestern airports and defined 3°latitude by 3°longitude boxes surrounding them. Background colors represent topography, with yellow corresponding to higher elevations. 13

2.2 Number of ACARS relative humidity measurements per LST-height bin, available in the Dallas area during JJA 2005-2014. 14

2.3 ACARS JJA cross-sections of relative humidity at (a) Dallas, (b) Houston, (c) Kansas City, (d) Tulsa, (e) Chicago, (f) St. Louis, (g) Phoenix and (h) Denver. Data from JJA of 2005 to 2014 are used. At the midwestern locations ((a)-(f)), the color bar ranges from 30% to 80% relative humidity. At the mountain locations ((g) and (h)), the color bar ranges from 20% to 70% relative humidity. Note the nocturnal relative humidity maxima between 2 km and 3 km from roughly 3 LST to 9 LST at the six midwestern airports. 16

2.4 ACARS JJA cross-sections of (a) specific humidity q [g/kg], (b) fractional q anomaly, calculated as $\frac{q(z,t)-\overline{q}(z)}{\overline{q}(z)}$, (c) temperature anomaly [K] and (d) lapse rate [K/km] at Dallas. 17

2.5 ACARS JJA cross-sections of (a) specific humidity q [g/kg], (b) fractional q anomaly, calculated as $\frac{q(z,t)-\overline{q}(z)}{\overline{q}(z)}$, (c) temperature anomaly [K] and (d) lapse rate [K/km] at Kansas City. 19

2.6 ACARS cross-sections of relative humidity during (a) DJF, (b) MAM, (c) JJA and (d) SON at Dallas. Note that nocturnal relative humidity maxima are strongest during JJA and persist into SON, but weaken. 20

2.7 Interannual variation in JJA vertical profiles of relative humidity near 5 LST at (a) Dallas, (b) Houston, (c) Kansas City, (d) Chicago over the ten-year period, 2005 to 2014. JJA of 2009 and 2011 show relative humidity maxima near 2.5 km at all locations. 22

2.8 JJA 2011 cross-sections of relative humidity at (a) Dallas, (b) Houston, (c) Kansas City, (d) Tulsa, (e) Chicago, (f) St. Louis, (g) Phoenix and (h) Denver. Note the strong presence of the nocturnal relative humidity maxima near 2.5 km at the six midwestern locations. 23

2.9 JJA 2014 cross-sections of relative humidity at (a) Dallas, (b) Houston, (c) Kansas City, (d) Tulsa, (e) Chicago, (f) St. Louis, (g) Phoenix and (h) Denver. Note that neither of the six midwestern locations have nocturnal relative humidity maxima above the boundary layer 24

2.10 Spatial and diurnal variation of JJA 750 hPa vertical winds [Pa/s] from MERRA-2. Data from JJA of 2005 to 2014 are used in order to be consistent with the ACARS time period. Note the daytime downward motion and nocturnal upward motion at each of the six midwestern sites. 26

2.11 JJA cross-sections of vertical winds [Pa/s] at (a) Dallas, (b) Houston, (c) Kansas City, (d) Tulsa, (e) Chicago, (f) St. Louis, (g) Phoenix and (h) Denver from MERRA-2. Data are averaged over JJA of 2005 to 2014. At the six midwestern sites, there is upward motion between 2 km and 3 km overnight. 27

2.12 Seasonal variation in 750 hPa vertical motion [Pa/s] at Dallas during 2011. The largest diurnal variation in vertical motion occurs during the summer months (May-August). 28

2.13 JJA cross-sections of MERRA-2 relative humidity at (a) Dallas, (b) Houston, (c) Kansas City, (d) Tulsa, (e) Chicago, (f) St. Louis, (g) Phoenix and (h) Denver during 2011. MERRA-2 underrepresents the nocturnal relative humidity maxima observed at 2.5 km in the Midwest. 29

2.14 JJA cross-sections of MERRA-2 relative humidity tendency [/hr] at Dallas associated with vertical motion. Panel (a) shows the relative humidity tendency after changes in q generated by vertical motion. Panel (b) shows the relative humidity tendency after changes in temperature generated by vertical motion. Panel (c) shows the relative humidity tendency after changes in both q and temperature. 32

2.15 JJA diurnal cross-sections of (a) MERRA-2 relative humidity anomaly at Dallas, associated with diurnal changes in q and T generated by vertical motion, and (b) observed relative humidity anomaly from ACARS. 33

2.16 JJA mean diurnal cross-sections of wind speed (a,b), u (c,d) and v (e,f) in the Dallas area from ACARS and MERRA-2 [m/s]. Data from 2005 to 2014 are used. The nocturnal LLJ maximum spans between 500 m and 900 m. The zonal direction of the LLJ switches from easterly to westerly near midnight. . 35

2.17 JJA hodographs [m/s] at Dallas from (a) ACARS and (b) MERRA-2. Here, points represent different local times and the colors represent different heights. Note the circular shape of each hodograph from both datasets. The larger the circle, the greater the diurnal variation of friction. 36

Abstract

Commercial aircraft measurements from the ACARS [Aircraft Communications Addressing and Reporting System] dataset were used to obtain the vertical variation of lower tropospheric relative humidity over the diurnal cycle. Relative humidity maxima were observed during the summer between 2 km and 3 km overnight at six airports in the American Midwest from roughly 3 LST to 9 LST. The nocturnal relative humidity maxima coincide with both positive anomalies in specific humidity and negative anomalies in temperature, as would be expected if the maxima were generated by upward motion. Spatial, diurnal and vertical variations of vertical winds from the MERRA-2 [Modern-Era Retrospective analysis for Research and Applications, Version 2] reanalysis dataset show that during the daytime in the lower troposphere, there is strong upward motion over the Rocky Mountains and downward motion over the Midwest. At night, the circulation reverses with upward motion over the Midwest that is strongest near 2 km in altitude, therefore coincident with the height and timing of the nocturnal relative humidity maxima. Several studies have indicated that this diurnal variation in vertical motion is induced by baroclinicity over sloping terrain, and is referred to as the mountain-plains solenoidal circulation. The relative humidity maxima are strongest during the summer and also show a high degree of interannual variability. The relative humidity maxima may be used as a diagnostic for the strength of the solenoidal circulation in climate models. The nocturnal Low Level Jet (LLJ) was also studied in relation to the relative humidity maxima. However, the LLJ was too low in altitude to be a main contributor to the maxima.

List of Abbreviations and Symbols Used

P_0	Surface pressure
Γ	-dT/dz, negative of vertical temperature gradient
Γ_d	Dry adiabatic lapse rate, 9.8K/km
ω	Pressure velocity
ω	Omega, pressure velocity
$\overline{q}(z)$	Diurnal mean specific humidity at a given height
ρ	Density
ACARS	Aircraft Communications Addressing and Reporting System
DJF	December-January-February, Meteorological winter
e	Vapour pressure
fractional anomaly in q	Difference between specific humidity at a given time and height and the diurnal mean specific humidity at that height, normalized by the diurnal mean specific humidity at that height
g	Acceleration due to gravity, $9.8m/s^2$
g/kg	Grams per kilogram
GESDISC	Goddard Earth Sciences Data and Information Services Centre
GPS	Global Positioning System
H	Pressure scale height
hPa	Hectopascal

JJA	June-July-August, Meteorological summer
K	Kelvin
K/km	Kelvin per kilometer
km	Kilometre
LLJ	Low Level Jet
LST	Local Solar Time
m/s	Meters per second
MADIS	Meteorological Assimilation Data Ingest System
MAM	March-April-May, Meteorological spring
MERRA-2	Modern-Era Retrospective analysis for Research and Applications, Version 2
NOAA	National Oceanic and Atmospheric Administration
P	Atmospheric Pressure
Pa/s	Pascals per second
PBL	Planetary Boundary Layer
q	Specific Humidity
RH	Relative humidity
SON	September-October-November, Meteorological fall
T	Temperature
u	Zonal wind component

UTC	Coordinated Universal Time
v	Meridional wind component
z	Height

Acknowledgements

First, I would like to thank Ian Folkins and Rachel Chang for their guidance and support during my time at Dalhousie. Their brilliant ideas and editing have greatly contributed to this work. I would also like to thank my committee members, Glen Lesins and Randall Martin for their input and ideas on this project. Finally, I would like to thank Brian Boys, Jeff Geddes, and Andy Morrow for their useful suggestions and/or help with Matlab.

The ACARS [Aircraft Communications Addressing and Reporting System] dataset was obtained through NOAA's MADIS [Meteorological Assimilation Data Ingest System] data archive. The MERRA-2 reanalysis dataset was accessed through the NASA GESDISC [Goddard Earth Sciences Data and Information Services Centre] archive.

Chapter 1

Introduction

The focus of the thesis is on the diurnal and vertical variation of lower tropospheric relative humidity in the American Midwest. We study the existence of anomalies in lower tropospheric relative humidity within the region and investigate possible forcings for these anomalies. This chapter provides background on the properties and dynamics of the Planetary Boundary Layer (PBL), and gives an overview of boundary layer processes that affect the tendency of relative humidity. We also discuss the diurnal cycle of rainfall in the American Midwest, and a regional scale thermal circulation called the mountain-plains solenoid. In Chapter 2, we present the details of the research project. Finally, in Chapter 3, we summarize the results from the project and discuss future directions for the work.

1.1 The Planetary Boundary Layer

1.1.1 Observing the depth of the PBL

The PBL is the lowest layer of the atmosphere where heat, moisture and momentum from the Earth's surface interact with free tropospheric air through turbulent motions. It is where surface heating, cooling and frictional effects are most significant. The top of the PBL is often characterized by a capping inversion or stable layer (Seidel et al. 2010). However, the height of the boundary layer has also been defined in relation to humidity (Seidel et al. 2010) and aerosol measurements (McGrath-Spangler and Denning 2013). These definitions include (i) a minimum vertical gradient in relative humidity (von Elgin and Teixeira 2013), or specific humidity (Seidel et al. 2010) and (ii) a maximum in aerosol backscatter (McGrath-Spangler and Denning 2013). The heights of each of these features are often inconsistent with the inversion height (Seidel et al. 2010).

Many types of measurements have been used to observe the depth of the PBL.

Vertical profiles in the lower troposphere have been obtained from radiosonde (Seidel et al. 2010; Schmid and Niyogi 2012; Liu and Liang 2010), LIDAR (McGrath-Spangler and Denning 2013), GPS (Guo et al. 2011; Chan and Wood 2013; Cheng-Ying et al. 2011), aircraft (Cheng-Ying et al. 2011), and reanalysis (von Elgin and Teixeira 2013) datasets. Seidel et al. (2010) used radiosonde data to obtain vertical profiles of temperature, potential temperature, relative humidity, specific humidity, and refractivity. They found that boundary layer height calculated from vertical profiles of humidity are generally higher than the heights determined using temperature measurements and attributed this discrepancy to low-level stratocumulus. McGrath-Spangler and Denning (2013) used aerosol backscatter measurements from space-borne LIDAR, however they found that this method is ineffective in the presence of thick, convective clouds. Also, sometimes aerosol gradients from the residual layer of a previous day can be detected, which can lead to higher estimations of PBL depth (McGrath-Spangler and Denning 2013). von Elgin and Teixeira (2013) found that PBL heights derived from vertical profiles of relative humidity agree best with the height of the capping inversion.

1.1.2 Diurnal and Seasonal Cycles of PBL Depth

The diurnal cycle of boundary layer height is forced by surface heating and cooling, as well as cloud cover (Garratt 1992). During the day, the depth of the PBL increases to a maximum, usually within a few kilometres of the surface. The diurnal maximum depth usually occurs near 15 LST (Liu and Liang 2010). After sunset, the convective boundary layer collapses to a thin layer near the surface, and radiative cooling of the surface stabilizes the layer from below. The depth of the nocturnal boundary layer is typically on the order of hundreds of meters (Liu and Liang 2010). Above the stable boundary layer, there remains a residual layer of air from the daytime convective boundary layer.

Over land, the PBL height is highest in summer over dry regions in the subtropics, where it can reach a depth of at least 3 km, and is lowest in winter near the Poles (von Elgin and Teixeira 2013). McGrath-Spangler and Denning (2013) found that the largest seasonal variability of PBL height occurs in the Sahara and Kalahari deserts, where variability in PBL heights can be as large as 1 km. However, over ocean and

coastal areas, seasonal variability is much weaker (McGrath-Spangler and Denning 2013; Seidel et al. 2010). With strong mixing in the ocean near the surface, and the ocean's large capacity to retain heat, diurnal and seasonal variations in sea surface temperature are therefore weak (Stull 1988).

1.1.3 Boundary Layer Relative Humidity

Relative humidity is defined as the ratio of the actual amount of water vapour in the air to the amount of water vapour required to achieve saturation at the same air temperature. There have been several studies on the global or spatial variability of relative humidity at the surface (Ruzmaikin et al. 2014; Dai 2006). Dai (2006) found that over land, surface relative humidity typically ranges from 70% to 80%, except 30% to 60% in desert regions.

Vertical profiles of relative humidity in the PBL have also been studied (Seidel et al. 2010; Liu and Liang 2010; Ek and Mahrt 1994). The tendency of relative humidity depends on changes in moisture and temperature. Surface evapotranspiration acts to increase boundary layer relative humidity, while upward eddy heat fluxes from the surface and entrainment of dry air from above the boundary layer reduce it (Ek and Mahrt 1994).

The top of the convective boundary layer can be observed by a vertical maximum in relative humidity (Ek and Mahrt 1994). In a well-mixed boundary layer, specific humidity q is assumed to be constant. Specific humidity is defined as the ratio of the mass of water vapour to the total mass of air and is proportional to $\frac{e}{P}$, where e is the vapour pressure and P is total pressure. Atmospheric pressure decreases exponentially with height following Equation 1.1

$$P = P_0 exp\left(\frac{-z}{H}\right) \tag{1.1}$$

where P_0 is the surface pressure, z is height, and H is a pressure scale height. In a mixed layer, pressure decreases slowly with height. Therefore, the vapour pressure must also decrease weakly with height. Relative humidity is defined as the ratio of the vapour pressure to the saturation vapour pressure, where the saturation vapour pressure at a given height depends on the air temperature at that height. Assuming lapse rates in the mixed layer are dry adiabatic, then the saturation vapour pressure

would decrease strongly with height compared to the vapour pressure. Therefore, relative humidity increases with height in a well-mixed boundary layer.

The vertical variation of lower tropospheric relative humidity over the full diurnal cycle is not well characterized. Zhang and Klein (2013) used Raman lidar data over a site in the Southern Great Plains to compare diurnal cycles of PBL relative humidity during days of deep convection and shallow cumulus. They found that relative humidity in the PBL is higher on days of deep convection. Ferrare et al. (2003) used lidar measurements to obtain a summer diurnal climatology of relative humidity near the same site. A limitation of using these intensive lidar campaigns is that data are not available for extended periods. In order to construct a diurnal climatology, several years of data are required. In addition, these lidar measurements are generally available at only one site.

The diurnal variation of boundary layer relative humidity has important interactions with convective precipitation, clouds, and turbulence. In order to accurately simulate the timing of convective weather, a realistic simulation of the boundary layer over the diurnal cycle is required. Also, convection affects the evolution of the boundary layer. For example, convective updrafts preferentially remove air with higher temperature and relative humidity, and convective downdrafts bring down cold dry air into the boundary layer (Zipser 1969). Additionally, in climate models, boundary layer relative humidity is often used within cloud parameterizations to help determine cloud condensate or cloud fraction (Teixeira 2001). The diurnal variation of boundary layer relative humidity can therefore be used to help determine whether climate models are simulating the diurnal variation of boundary layer clouds in a physically consistent manner. Finally, observations of the diurnal and vertical variation of relative humidity can be used to test aspects of the parameterizations of boundary layer mixing. These include the diurnal variation of mixed layer depth and the turbulent fluxes of moisture and heat.

1.1.4 Nocturnal Low Level Jet

The nocturnal Low Level Jet (LLJ) is an overnight maximum in wind speed with respect to height, that is typically observed within 1 km of the Earth's surface. The height of the LLJ has been observed within 100 m (A.Karipot et al. 2009) of the

ground or sometimes as high as 900 m (Stull 1988). The nocturnal LLJ has been studied extensively over the U.S. Great Plains (Berg et al. 2015; Klein et al. 2015; Song et al. 2005; Bonner 1968; Blackadar 1957). However, the LLJ has also been observed over the Eastern U.S. (A.Karipot et al. 2009; Sjostedt et al. 1990), the Netherlands (Baas et al. 2009), and Africa (Nicholson 2016). In the Great Plains, wind maxima as high as 32 m/s have been observed in the LLJ core (Wu and Raman 1998).

During the daytime, there is an approximate three-way balance between the pressure gradient force, the coriolis force, and friction (Holton 2004). At sunset, the convective boundary layer collapses, restricting frictional deceleration to a shallow layer near the surface. Above this layer, there remains an imbalance between the pressure gradient and coriolis forces, and the winds accelerate, becoming super-geostrophic. The wind vector then rotates about the geostrophic wind vector in an inertial oscillation (Blackadar 1957). The inertial oscillation theory, however does not specify why the nocturnal LLJs occur more frequently in preferred geographic locations. For example, Bonner (1968) found a maximum frequency of occurrence of nocturnal LLJs over the U.S. Southern Great Plains, specifically near the Kansas-Oklahoma border.

The development of the nocturnal LLJ over the Great Plains has also been explained by orographic effects. Overnight, differential radiative cooling over sloping terrain creates a horizontal temperature gradient between the mountains and the plains (Stull 1988). This creates vertical shear in the horizontal winds and a LLJ forms during the overnight hours. During the daytime, the stronger winds in the LLJ tend to mix with the slower moving air below, reducing the strength of the jet.

The nocturnal LLJ is also known as a mechanism of moisture transport to the American Midwest. Wind directions in the LLJ core are typically southerly during the warm seasons (Bonner 1968; Wu and Raman 1998). The northward transport of moisture from the Gulf of Mexico contributes to the development of nocturnal thunderstorms over the Midwest (Higgins et al. 1997; Wu and Raman 1998; Pitchford and London 1962).

1.2 Climatological features of interest in the American Midwest

1.2.1 Diurnal Cycle of Rainfall

The diurnal cycle of rainfall in the American Midwest has been of great interest in the literature. Many studies have observed a nocturnal peak in rainfall over the Central U.S. during the summer months (Balling 1985; Tuttle and Davis 2006; Carbone and Tuttle 2008; Geerts et al. 2016; Reif and Bluestein 2017). About half of the total nocturnal summer rainfall over this area is associated with eastward propagating convective rainfall from the Rocky Mountains (Jiang et al. 2006). Li and Smith (2010) showed that in the 36°N to 44°N latitude range, convective rainfall is initiated in late afternoon near the Rocky Mountains, and then propagates eastward toward the Midwest overnight. They suggested that this rainfall is triggered by potential vorticity anomalies generated above the Rocky Mountains. These anomalies are subsequently advected eastward, and trigger convective precipitation by induced ascent in the lower troposphere. The generation of these potential vorticity anomalies is expected to arise from daytime heating over elevated terrain (Li and Smith 2010).

The nocturnal LLJ has also been studied in relation to the nocturnal rainfall peak (Pu and Dickinson 2014; Monaghan et al. 2010). As mentioned in Section 1.1.3, the LLJ is a moisture source to the Midwest (Wu and Raman 1998; Higgins et al. 1997). Moisture is a necessary ingredient for convective rainfall initiation.

Finally, several studies have indicated the presence of a regional scale circulation called the mountain-plains solenoid. Vertical winds, represented in reanalysis datasets over the continental U.S. have shown that during the daytime, there is upward motion over the Rocky mountains, and widespread downward motion over the Midwest (Tuttle and Davis 2013; Carbone and Tuttle 2008; Trier et al. 2010). At night, there is a reversal in the vertical motion field, with downward motion over the mountains, and widespread upward motion over the Midwest. The nocturnal upward motion over the Midwest is expected to be related to the observed nocturnal rainfall peak in the region (Tuttle and Davis 2013; Carbone and Tuttle 2008; Trier et al. 2010). The diurnal evolution of the solenoidal circulation will be discussed in more detail in the next section.

1.2.2 The Mountain-Plains Solenoid

During the daytime, solar heating of mountainous regions creates a horizontal temperature gradient over the eastern slopes, as air over the mountains is warmer than air over the plains at the same height above sea level. This creates a horizontal pressure gradient over the sloping terrain and an easterly (upslope) flow. Aloft, the air is transported eastward, and then subsides over the plains. This thermal circulation is often called the mountain-plains solenoid. The term solenoid refers to the development of the vertical circulations in response to baroclinicity over the sloping terrain. In a baroclinic environment, pressure and density surfaces intersect. The circulation pattern described is an attempt to align the isobars and the isopycnals, or in other words create a more barotropic environment.

The mountain-plains solenoid has mainly been studied through model simulations (Tripoli and Cotton 1989; Wolyn and McKee 1994; Bossert et al. 1989). Tripoli and Cotton (1989) studied the initiation of a mesoscale convective system in the western plains in relation to the mountain-plains solenoid. During the early morning, surface heating erodes the nocturnal inversion from below. This allows the ambient westerly momentum above the inversion to mix down to the surface. Upslope winds associated with differential solar heating between the mountains and the plains, converge with the ambient westerlies (Tripoli and Cotton 1989; Wolyn and McKee 1994). This lee side convergence zone is a favourable region for the initiation and development of mesoscale convective systems (Tripoli and Cotton 1989; Banta 1984). Wolyn and McKee (1994) simulated the development of the mountain-plains solenoid and performed sensitivity tests to investigate interactions between the solenoidal circulation and the ambient flow. They found that the evolution of the solenoid is sensitive to the amount of solar heating and that the circulation is strongest on days near the summer solstice about 5 hours after sunset (when the boundary layer is less stable). The solenoid is also stronger when the ambient westerly winds are weaker and soil moisture is lower.

Aspects of the mountain-plains solenoid have been observed through radiosonde or aircraft soundings (Tripoli and Cotton 1989; Wolyn and McKee 1994; Banta 1984), surface observations (Banta 1984), and reanalysis representations of vertical motion (Carbone and Tuttle 2008; Tuttle and Davis 2013; Trier et al. 2010). Banta (1984)

observed upslope winds at a mountain base during the late morning and into the early afternoon. Sullivan et al. (2016) studied a relationship between the mountain-plains solenoidal circulation and ozone pollution along the Colorado Front Range, using wind profiler, aircraft, sonde, and surface measurements. They found that daytime upslope flow associated with the solenoidal circulation can lead to an accumulation of ozone in the boundary layer along the foothills. Also, the returning westerly flow aloft is a mechanism of transporting boundary layer pollutants over the mountains into the free troposphere over the plains (Sullivan et al. 2016).

1.3 Atmospheric Tides and Surface Pressure Perturbations

The absorption of solar radiation by the earth's atmosphere excites gravity waves with diurnal and semidiurnal periods. The amplitude and period of the waves has been observed through perturbations in surface pressure (Dai and Wang 1999), temperature, and wind speed (Lindzen and Chapman 1970). There is both a diurnal oscillation and a semidiurnal oscillation in surface pressure (Lindzen and Chapman 1970). Dai and Wang (1999) found that both pressure oscillations are similar in magnitude over most latitudes, and that the diurnal oscillation in pressure is strong in mountainous regions (roughly 1.1 mb), peaking between 10 LST and 12 LST in the midlatitudes (Dai and Wang 1999). The diurnal oscillation in pressure is more sensitive to land-sea contrasts than the semidiurnal circulation, and the semidiurnal oscillation peaks at roughly 10 LST and 22 LST in the midlatitudes (Dai and Wang 1999). These oscillations in surface pressure would be expected to be associated with oscillations in the vertical motion field.

Chapter 2

Nocturnal Relative Humidity Maxima above the Boundary Layer in the American Midwest: A Diagnostic for the Mountain-Plains Solenoidal Circulation

Authors: Amanda Mercer, Rachel Chang, and Ian Folkins
Department of Physics and Atmospheric Science, Dalhousie University, Halifax, NS, Canada

2.1 Abstract

Measurements from the ACARS [Aircraft Communications Addressing and Reporting System] dataset between 2005 and 2014 are used to construct diurnal vertical cross-sections of relative humidity in the lower troposphere at six airports in the American Midwest. In summer, relative humidity maxima occur between 2 km and 3 km during the overnight hours of 3 LST to 9 LST. These maxima coincide with negative anomalies in temperature and positive anomalies in specific humidity. Vertical winds from the MERRA-2 [Modern-Era Retrospective analysis for Research and Applications, Version 2] reanalysis dataset show that the height and diurnal timing of these positive relative humidity anomalies are consistent with the regional diurnal pattern of vertical motion. During the day, there is rising motion over the Rocky Mountains and subsidence over the Midwest, while conversely at night, there is sinking motion over the Mountains and rising motion over the Midwest. The nocturnal relative humidity maxima over the Midwest are the strongest direct observational evidence to date of this mountain-plains solenoidal circulation, and provide a useful diagnostic for testing the strength of this circulation in climate and reanalysis models. There is significant interannual variability in the strength of the nocturnal relative humidity maxima. In 2011, the relative humidity maxima are very pronounced. In 2014, however, they are almost non-existent. Finally, the relative humidity maxima

are discussed in relation to the Low Level Jet (LLJ). The LLJ appears to be too low to directly contribute to the nocturnal relative humidity maxima.

2.2 Motivation

Boundary layer turbulence is mainly generated by low level wind shear and convective instability, and usually gives rise to an upward eddy moisture flux from the surface. Due to the requirement that potential temperature increase with height in a stable atmosphere, strong boundary layer turbulence also tends to cool the upper part of a well mixed boundary layer. The combination of these turbulent moisture and heat fluxes tends to decrease relative humidity near the surface, and increase relative humidity in the upper part of the boundary layer. Observations of the diurnal and vertical variation of relative humidity within the boundary layer are therefore an important diagnostic of the strength of boundary layer turbulence, and of the propensity of a boundary layer to support cloud development.

The diurnal variation of relative humidity in the lower troposphere can also be used to diagnose the existence of diurnal changes in large scale vertical motion. These motions can be generated by tidal circulations, sea breeze circulations, or circulations generated by orographic heating. Several modelling studies have indicated the presence of a large scale diurnal variation in vertical motion in the American Midwest, sometimes called the mountain-plains solenoid, that is associated with the diurnal variation in heating over the Rocky Mountains (Tripoli and Cotton 1989; Wolyn and McKee 1994). The term "solenoid" refers to the vertical circulations that develop in response to baroclinic environments over sloping terrain. Wolyn and McKee (1994) used a two-dimensional numerical model to simulate the daytime evolution of the mountain-plains solenoid, and to investigate interactions between the mountain-plains solenoid and the background environment. They found that the strength of the mountain-plains solenoid was sensitive to soil moisture, the strength of the ambient winds (westerlies), and solar heating (Wolyn and McKee 1994). Tripoli and Cotton (1989) simulated the growth of a mesoscale convective system in response to the mountain-plains solenoid.

While there have been several simulations of the mountain-plains solenoid, there is a lack of direct observational evidence of this circulation. Radiosonde data has been

used to observe vertical variations in horizontal wind and temperature near the Rockies (Tripoli and Cotton 1989; Wolyn and McKee 1994; Bossert et al. 1989). However, radiosondes are typically launched at 2 standard times per day, and cannot fully capture diurnal variability. The mountain-plains solenoidal circulation is known to affect air quality. Ozone measurements have shown that the circulation is a mechanism that contributes to ozone exceedences along the Colorado Front Range, and that it is a way of exporting boundary layer pollutants into the free troposphere (Sullivan et al. 2016). The vertical motion associated with the mountain-plains solenoid is represented in reanalysis datasets (Carbone and Tuttle 2008; Tuttle and Davis 2013). Tuttle and Davis (2013) show the expected daytime upward motion over the Rocky Mountains and downward motion over the plains, due to solar heating of elevated terrain. Overnight, there is a reversal in the vertical motion field with subsidence over the mountains and upward motion over the plains (Tuttle and Davis 2013; Carbone and Tuttle 2008). The nocturnal upward motion over the plains appears to be related to the observed nocturnal rainfall in the region (Carbone and Tuttle 2008; Trier et al. 2010; Zhang et al. 2014). This upward motion would also be expected to enhance relative humidity in the lower troposphere. However, observations of lower tropospheric relative humidity have not yet been directly studied in relation to this circulation.

We use commercial aircraft measurements from the Aircraft Communications Addressing and Reporting System (ACARS) (Moninger et al. 2003) to characterize the diurnal and vertical variation of lower tropospheric relative humidity at six midwestern, and two mountain airports. This data is continuously available from July 2001 to the present, and has reasonably good coverage throughout the boundary layer. We focus on overnight relative humidity maxima that are observed near 2.5 km during the summer. Section 2.3 describes the ACARS and other datasets used. Section 2.4 shows diurnal vertical cross-sections of relative humidity at the eight sites during the summer from 2005 to 2014. We also show diurnal cross-sections of temperature and specific humidity at Dallas and Kansas City. Section 2.5 discusses the interannual variability of the lower tropospheric relative humidity anomalies. In Section 2.6, we show the spatial and diurnal variation of 750 hPa vertical motion, as well as mean vertical cross-sections of vertical motion, from MERRA-2 reanalysis data. Finally,

the nocturnal Low Level Jet (LLJ) is an important source of moisture to the Midwest (Berg et al. 2015; Pitchford and London 1962; Higgins et al. 1997). Section 2.7 discusses the direction and height of the LLJ in relation to overnight relative humidity anomalies. At most midwestern locations, the LLJ is below 2 km. It is therefore not expected to directly contribute to the 2.5 km nocturnal relative humidity maxima.

2.3 Data Sets

2.3.1 Meteorological data from commercial aircraft

The ACARS dataset (Moninger et al. 2003) is stored within the Meteorological Assimilation Data Ingest System (MADIS), run by the National Oceanic and Atmospheric Administration (NOAA). The dataset includes measurements of aircraft location, altitude, time of day, temperature, dew point temperature, relative humidity, wind speed and wind direction. Data are available from July 2001 to the present.

We focus on data collected during landings and takeoffs at eight airports during 2005-2014. These airports are: (i) Phoenix, AZ, (ii) Denver, CO, (iii) Houston, TX, (iv) Dallas, TX, (v) Tulsa, OK, (vi) Kansas City, MO, (vii) St. Louis, MO, and (viii) Chicago, IL. These sites were chosen because they have a larger volume of data and greater diurnal coverage than other midwestern and mountain locations. We define 3°latitude by 3°longitude boxes surrounding each airport. These boxes, as well as the airport locations (dots) are shown in Figure 2.1. Aircraft data within each box are assigned to 200 m altitude and hourly local solar time bins. Outliers within each airport box and time-height bin are detected and screened out according to the interquartile range rule. The interquartile range represents the spread of the middle 50% of data. It is defined as the difference between the upper and lower quartiles of data. Measurements that fall more than 1.5 times the interquartile range lower in magnitude than the lower quartile or higher in magnitude than the upper quartile are detected and screened out. After this screening process, the remaining data in each box and time-height bin are averaged over each month of each year. Local solar time (LST) is calculated from observed time of day (UTC) and longitude.

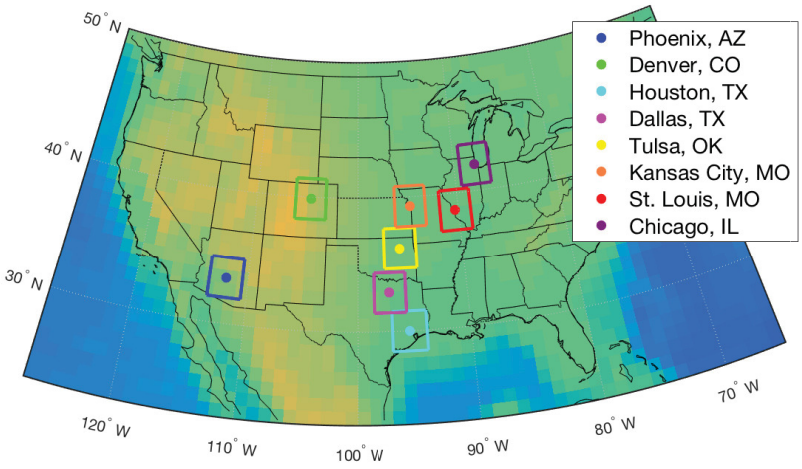

Figure 2.1: Map of midwestern airports and defined 3°latitude by 3°longitude boxes surrounding them. Background colors represent topography, with yellow corresponding to higher elevations.

To visualize the diurnal coverage in ACARS data, Figure 2.2 shows a contour plot indicating the number of June-July-August (JJA) relative humidity measurements available in Dallas over the years 2005-2014 within each LST-altitude bin. Between 5 LST and 22 LST, there are usually between 500 and 2000 measurements per hour within a 200 m height bin. During the overnight hours from 22 LST to 4.5 LST, the coverage is much less, with typically fewer than 200 measurements per hour within a 200 m height bin.

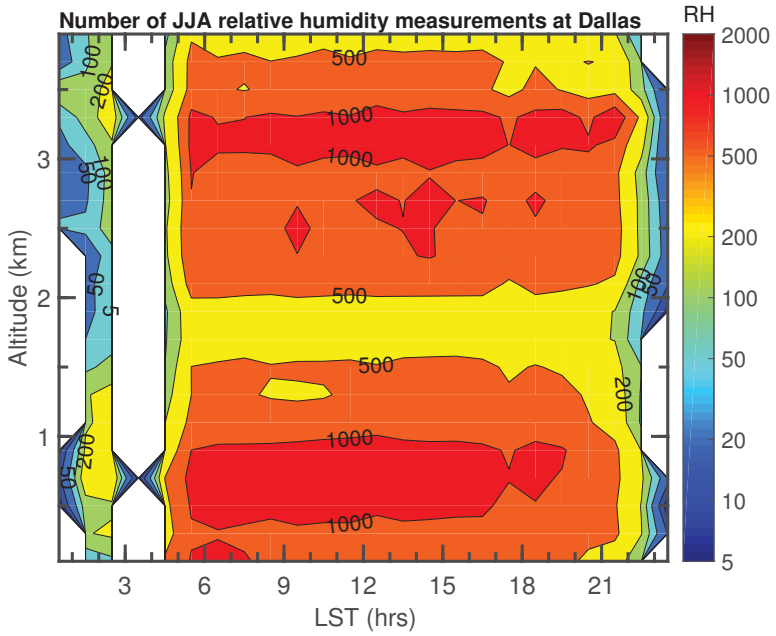

Figure 2.2: Number of ACARS relative humidity measurements per LST-height bin, available in the Dallas area during JJA 2005-2014.

There have been efforts by various government agencies to implement quality control on the ACARS data for use in numerical weather prediction models (Moninger et al. 2003). The accuracy of ACARS temperature and wind data over western and central U.S. has also been tested through collocation statistics (Benjamin et al. 1999). They determined the error in boundary layer temperature and winds to be 0.72 K and 2.5 m/s, respectively. ACARS temperature and wind measurements at Denver have also been tested through rawinsonde comparison (Schwartz and Benjamin 1995). They determined average differences of 0.59 K and 4 m/s for temperature and wind respectively, within a 25 km distance. Additionally, dew point temperature data from ACARS have been compared to radiosonde data over the continental U.S. (Mamrosh et al. 2002). They estimated an average dew point difference of 1.9 K within a 50 km distance.

2.3.2 Vertical Motion from MERRA-2 Reanalysis

The Modern-Era Retrospective analysis for Research and Applications, Version 2 (MERRA-2) reanalysis data (Gelaro et al. 2017) are managed by the NASA Goddard

Earth Sciences (GES) Data and Information Services Centre (DISC). The assimilated meteorological data lies on a 0.5°latitude by 0.625°longitude grid, with a 3-hour temporal resolution and 42 vertical levels. MERRA-2 assimilates in-situ and satellite observations (McCarty et al. 2016).

We used the three-dimensional assimilated meteorological fields (GMAO 2015) dataset, which includes vertical motion and relative humidity data. To be consistent with the ACARS time period, we focus on JJA data from 2005 to 2014.

2.4 Nocturnal relative humidity maxima above the boundary layer

We used the ACARS measurements to construct cross-sections of the mean diurnal variation of lower tropospheric relative humidity at each of the eight airport locations shown in Figure 2.1. These diurnal vertical cross-sections are shown in Figure 2.3. Each cross-section was constructed from measurements during JJA from 2005 to 2014. For each month, measurements are averaged within time-height bins. Each monthly climatology is given an equal contribution to the overall summer climatology over the ten years. White spaces indicate that there is no data within a time-height bin or that the data has been screened out. Averages are not calculated within a given time-height bin if there are less than 15 good measurements in total over the 10 summers.

Cross-sections from the six midwestern airport locations (i.e. excluding Phoenix and Denver) are broadly similar. They show a relative humidity minimum near the surface during the day and higher relative humidity near the surface at night. The nocturnal layer of higher relative humidity near the surface is lifted off the surface during the daytime, peaking between 1.5 km and 2 km near 15 LST. In addition, seven of the eight locations show a relative humidity maximum between 2 km and 3 km above the surface during the early morning hours (roughly 3 LST to 9 LST). At Denver, a relative humidity maximum 2 km to 4 km above the surface (i.e. 4 km to 6 km above sea level) appears in the late afternoon and persists after sunset.

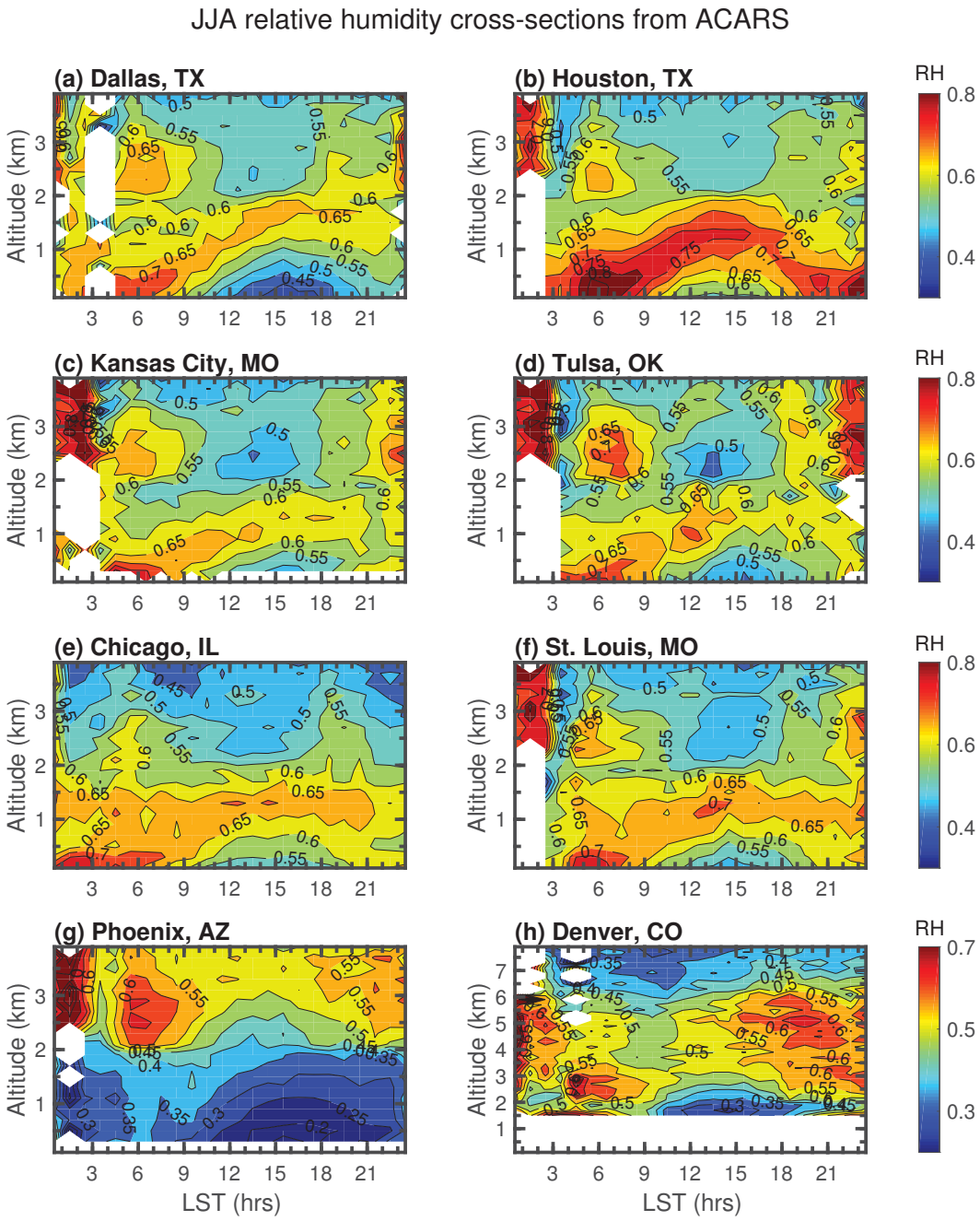

Figure 2.3: ACARS JJA cross-sections of relative humidity at (a) Dallas, (b) Houston, (c) Kansas City, (d) Tulsa, (e) Chicago, (f) St. Louis, (g) Phoenix and (h) Denver. Data from JJA of 2005 to 2014 are used. At the midwestern locations ((a)-(f)), the color bar ranges from 30% to 80% relative humidity. At the mountain locations ((g) and (h)), the color bar ranges from 20% to 70% relative humidity. Note the nocturnal relative humidity maxima between 2 km and 3 km from roughly 3 LST to 9 LST at the six midwestern airports.

Positive anomalies in relative humidity can arise from positive anomalies in specific humidity q. Figures 2.4 (a) and (b) show JJA mean diurnal cross-sections of q and the fractional anomaly in q at Dallas. Specific humidity was derived from aircraft measurements of dew point temperature and pressure-altitude. At a given height, the fractional anomaly in q was defined as the deviation from the 24 hour average normalized by the 24 hour average. Figure 2.4 (a) shows that the q contours tilt upward in the morning and early afternoon, and generate a strong positive q anomaly between 1 km and 2 km during the day. This is presumably the result of upward turbulent transport of moisture during the day. There is also a positive q anomaly overnight between 2 km and 2.5 km.

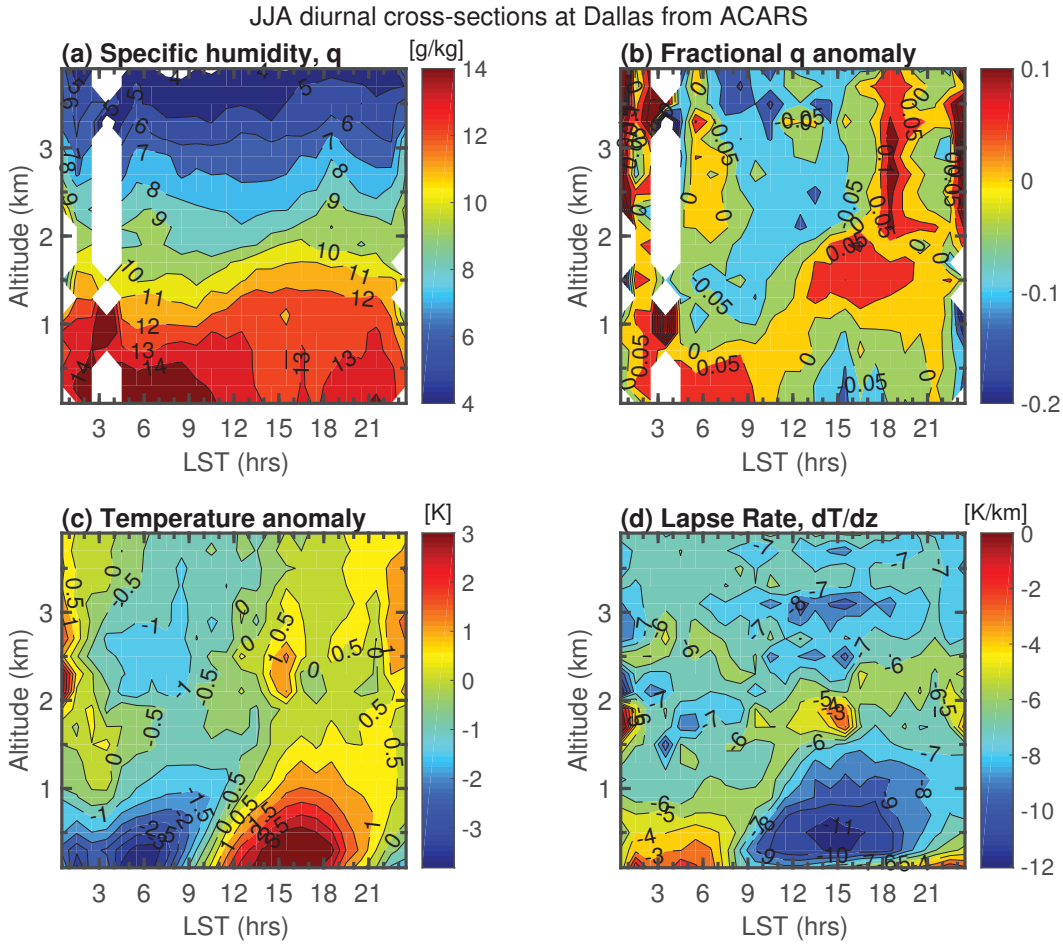

Figure 2.4: ACARS JJA cross-sections of (a) specific humidity q [g/kg], (b) fractional q anomaly, calculated as $\frac{q(z,t)-\overline{q}(z)}{\overline{q}(z)}$, (c) temperature anomaly [K] and (d) lapse rate [K/km] at Dallas.

Temperature anomalies can also contribute to relative humidity anomalies. Figure 2.4 (c) shows the JJA lower tropospheric diurnal temperature anomalies at Dallas. There is a positive temperature anomaly starting at the surface in late morning. The vertical tilt of the anomaly presumably reflects the upward transport of sensible heat from the surface. After sunset, there is a negative temperature anomaly near the surface. The negative temperature anomaly between 2 km and 3 km from 3 LST to 9 LST is coincident with the overnight relative humidity maximum at Dallas. The overnight positive relative humidity anomaly between 2 km and 3 km at Dallas is therefore associated with both a negative anomaly in temperature and a positive anomaly in specific humidity.

Figure 2.4 (d) shows Dallas JJA mean diurnal cross-sections of lapse rate (here dT/dz). Lapse rates are calculated from the mean temperature cross-sections. Overnight, the stable boundary layer (SBL) is indicated by the more stable lapse rates near the surface. By afternoon, there is a stable layer ("inversion") at a height of 2 km. This is coincident with the height of the daytime relative humidity maximum from Fig. 2.3 (a). Below the daytime capping stable layer, unstable lapse rates occur in the convective boundary layer.

Figure 2.5 shows diurnal climatological cross-sections of q, q anomaly, temperature anomaly and lapse rate at Kansas City. The overall patterns are quite similar to Dallas. Again, there is both a positive q anomaly and a negative temperature anomaly overnight between 2 km and 3 km, so that the nocturnal relative humidity maximum can again be attributed to both a decrease in temperature and an increase in q. In Fig. 2.5 (c), the diurnal variation in temperature between 2 and 3 km is almost as strong as the diurnal temperature variation near the ground. In Fig. 2.5 (d), the inversion at the top of the daytime boundary layer is stronger at Kansas City than at Dallas and forms earlier in the morning.

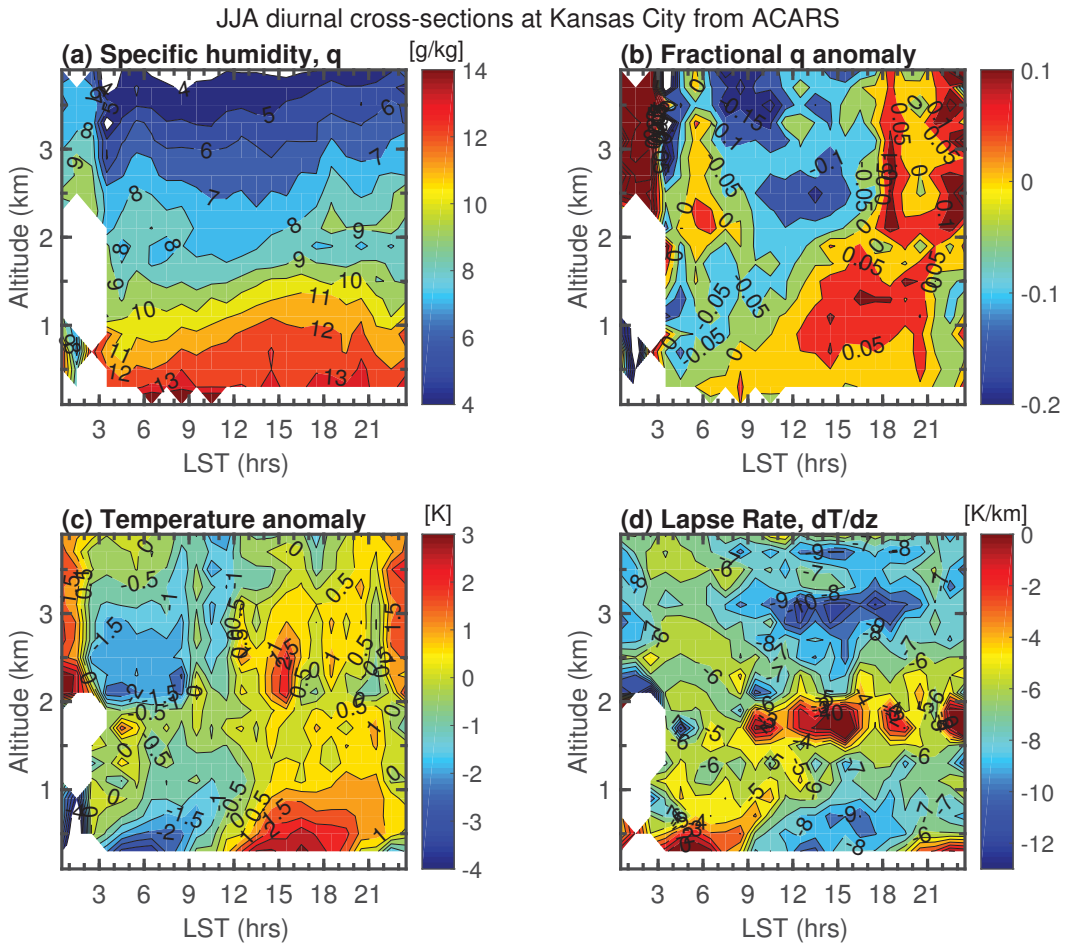

Figure 2.5: ACARS JJA cross-sections of (a) specific humidity q [g/kg], (b) fractional q anomaly, calculated as $\frac{q(z,t)-\bar{q}(z)}{\bar{q}(z)}$, (c) temperature anomaly [K] and (d) lapse rate [K/km] at Kansas City.

Figure 2.6 shows the seasonal variation of lower tropospheric relative humidity at Dallas. The daytime relative humidity maximum near the top of the boundary layer is strongest during the summer (JJA) and weakest during the winter (DJF). It is also highest in altitude during the summer and lowest in altitude during the winter. The 2-3 km overnight relative humidity maximum is strongest during the summer, but is present to some degree in the fall (SON).

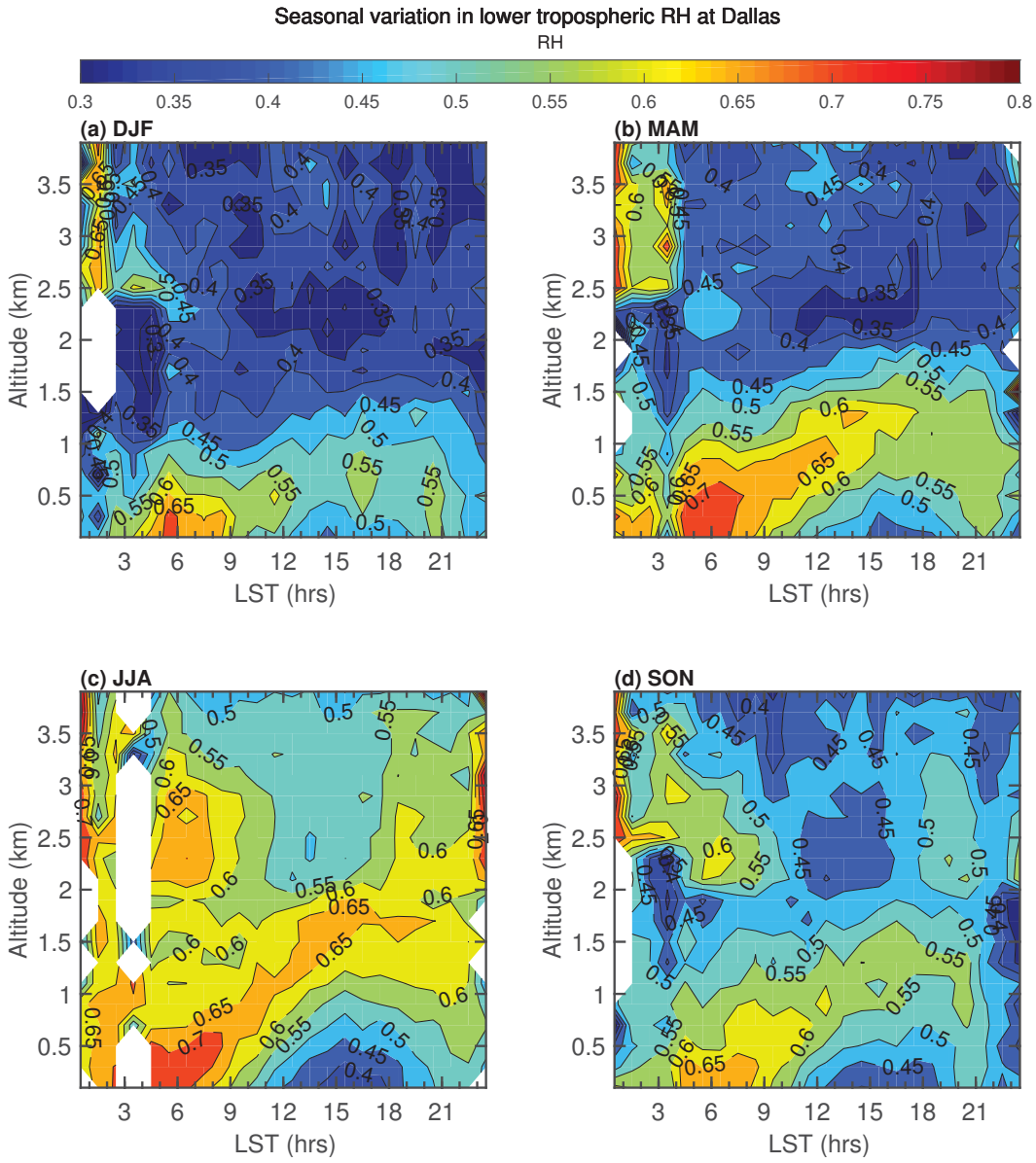

Figure 2.6: ACARS cross-sections of relative humidity during (a) DJF, (b) MAM, (c) JJA and (d) SON at Dallas. Note that nocturnal relative humidity maxima are strongest during JJA and persist into SON, but weaken.

2.5 Interannual variability in lower tropospheric relative humidity

Figure 2.7 shows that the nocturnal relative humidity maxima have significant interannual variability. It shows the JJA mean 5 LST relative humidity profile at four midwestern airports for individual years between 2005 and 2014. Each year in the ten-year period is represented by a different color. At Dallas, Houston and Kansas City, the 2-3 km nocturnal relative humidity maximum is strongest in 2011 (red), 2010 (orange), and 2009 (yellow). In the remaining years, it is only weakly present, if at all. At Chicago, the relative humidity maxima are weaker than at the other three locations.

Figure 2.8 shows JJA diurnal vertical cross-sections of relative humidity at each airport location during 2011. This is the year with the strongest 2-3 km nocturnal relative humidity maxima. They are present at all seven locations other than Denver, and appear to start at 18 LST. At Denver, there is again a late afternoon maximum between 4 km and 6 km.

For comparison, Figure 2.9 shows 2014 JJA diurnal vertical cross-sections of relative humidity at the same locations. The nocturnal 2-3 km relative humidity maximum is not present at any of the six midwestern locations or Phoenix. The fact that the nocturnal relative humidity maxima vary coherently in 2011 and 2014 across the midwestern airports suggests that they are associated with a large scale circulation.

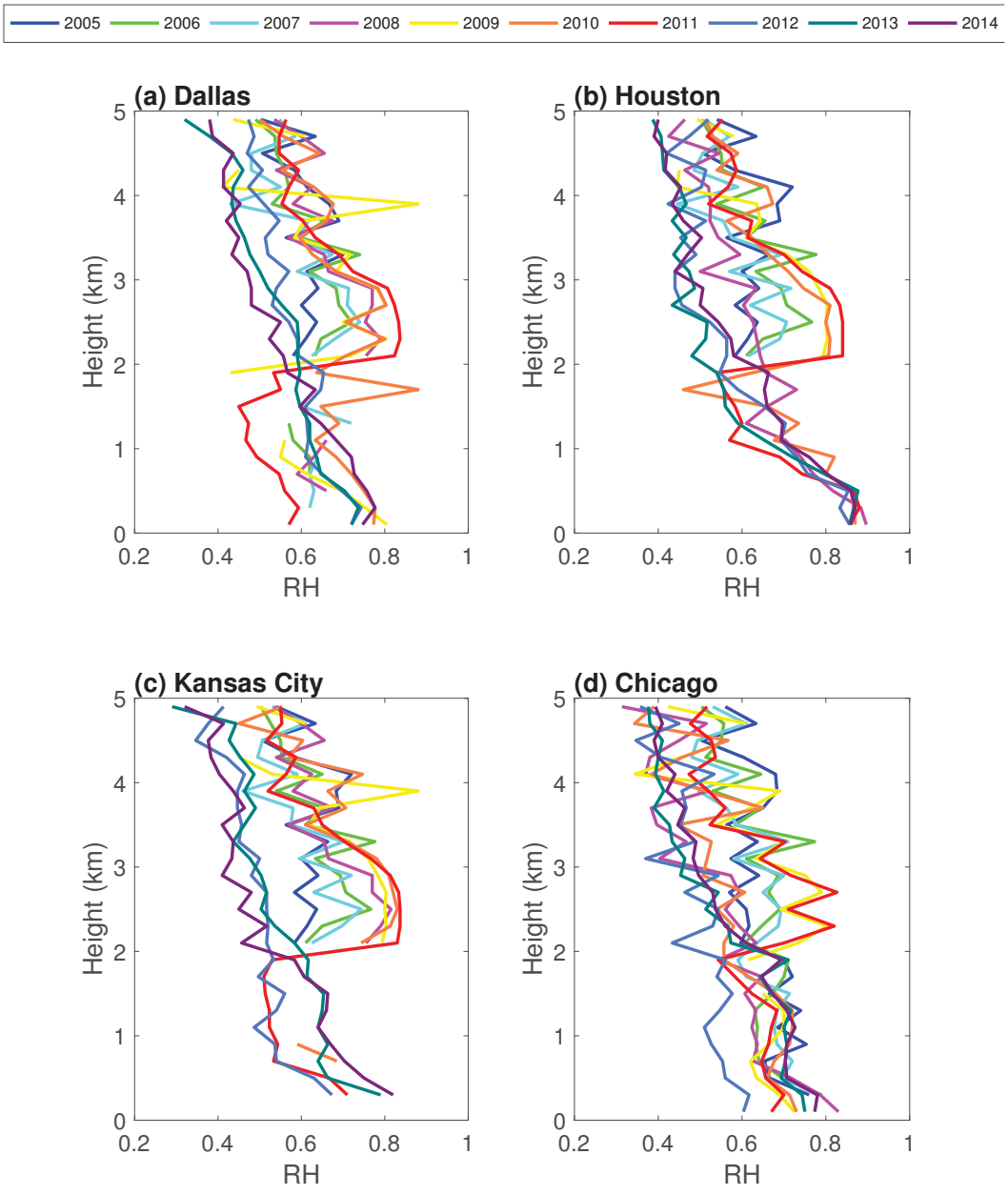

Figure 2.7: Interannual variation in JJA vertical profiles of relative humidity near 5 LST at (a) Dallas, (b) Houston, (c) Kansas City, (d) Chicago over the ten-year period, 2005 to 2014. JJA of 2009 and 2011 show relative humidity maxima near 2.5 km at all locations.

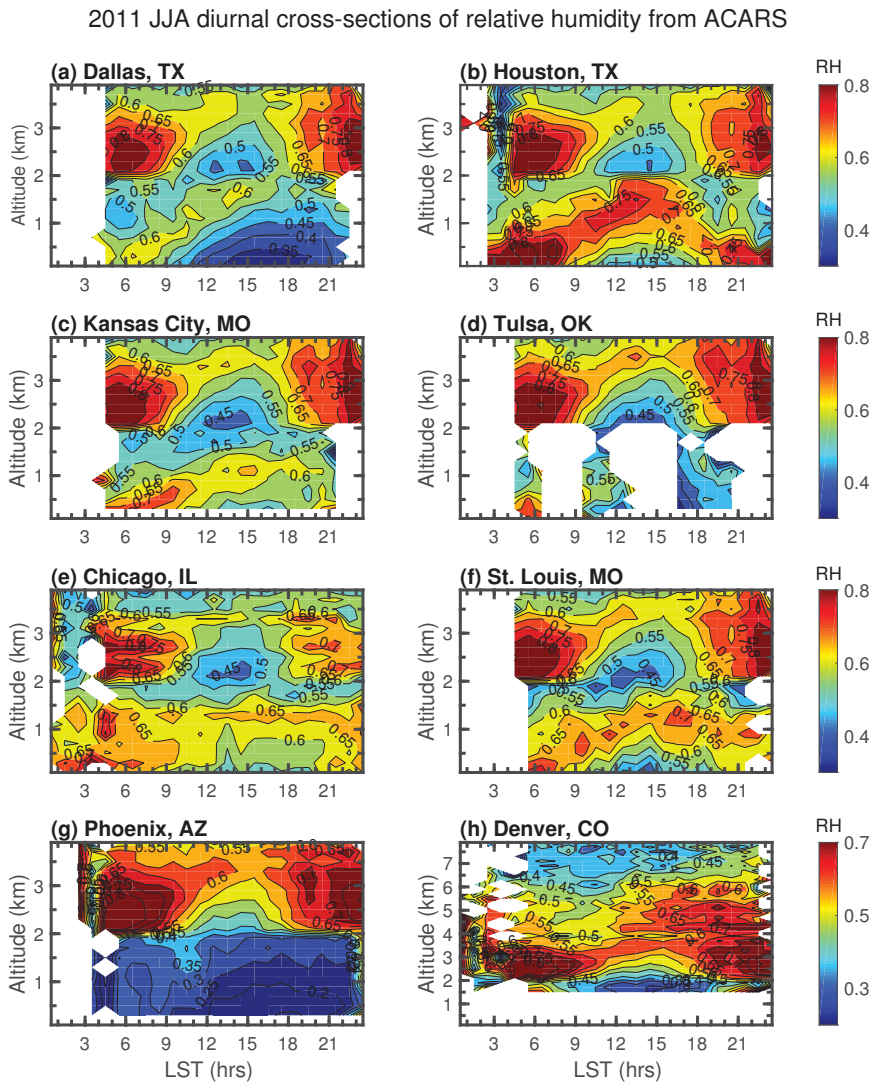

Figure 2.8: JJA 2011 cross-sections of relative humidity at (a) Dallas, (b) Houston, (c) Kansas City, (d) Tulsa, (e) Chicago, (f) St. Louis, (g) Phoenix and (h) Denver. Note the strong presence of the nocturnal relative humidity maxima near 2.5 km at the six midwestern locations.

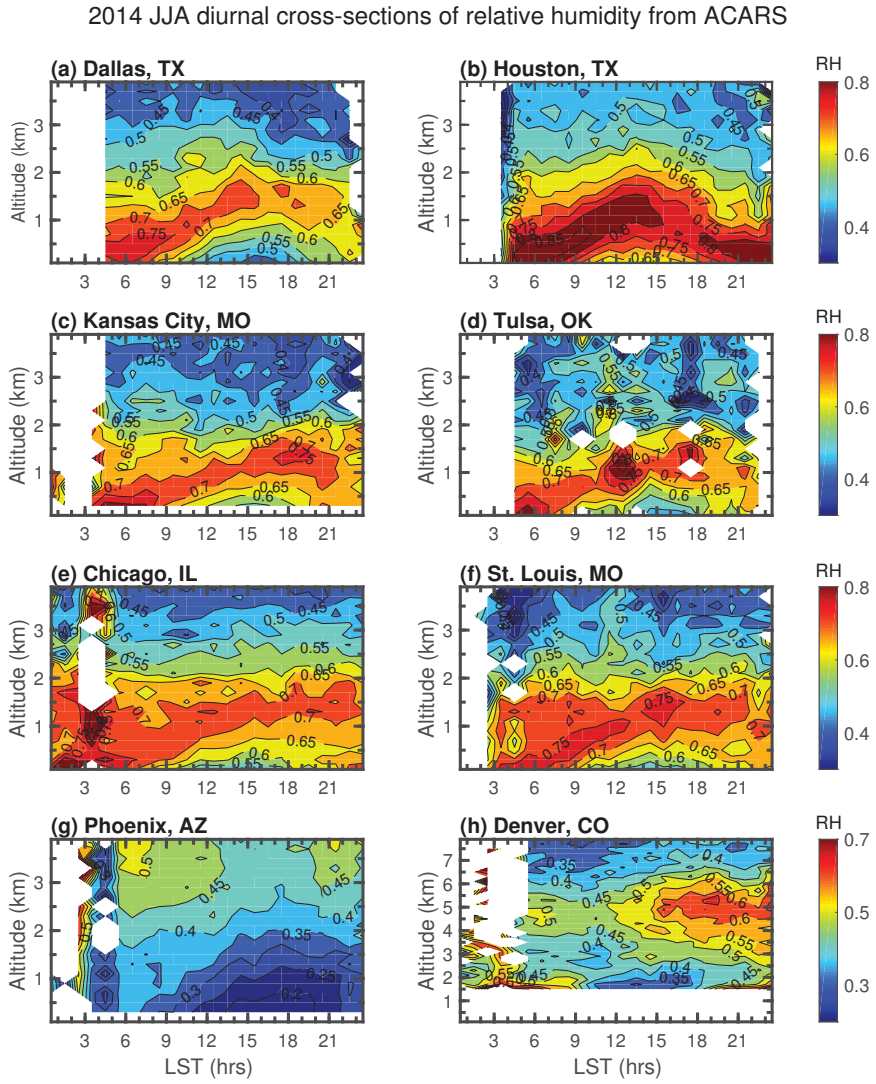

Figure 2.9: JJA 2014 cross-sections of relative humidity at (a) Dallas, (b) Houston, (c) Kansas City, (d) Tulsa, (e) Chicago, (f) St. Louis, (g) Phoenix and (h) Denver. Note that neither of the six midwestern locations have nocturnal relative humidity maxima above the boundary layer

2.6 MERRA-2 vertical motion and relative humidity

The vertical motion associated with the mountain-plains solenoid is likely to affect the diurnal variation in lower tropospheric relative humidity. We use MERRA-2 reanalysis data to show the spatial and diurnal variation of 750 hPa vertical motion over the continental U.S. Figure 2.10 shows the spatial variation of 750 hPa vertical motion every three hours, within the 28-45°N, 115-75°W domain, using JJA data from 2005 to 2014. Coastlines are outlined in black. The eight airport locations are labelled in white.

Here, we reference the local solar time (LST) to 97°W. At 14.5 LST, 17.5 LST and 20.5 LST, there is upward motion over the mountains (blue) and widespread downward motion over the plains (red). The downward motion over the plains is strongest at 17.5 LST and 20.5 LST. Overnight, at 2.5 LST, 5.5 LST and 8.5 LST, there is downward motion over the mountains and widespread upward motion over the plains. Upward motion over the plains is strongest at 2.5 LST.

Figure 2.11 shows diurnal cross-sections of vertical motion at each of the eight airport locations during JJA of 2005 to 2014, using data from the nearest 0.5°latitude by 0.625°longitude grid box to each airport. The six midwestern airport locations have broadly similar diurnal patterns. During the afternoon and evening, there is downward motion that is strongest near 2 km. Overnight, there is upward motion between 2 km and 3 km. This upward motion is coincident with the height and timing of the relative humidity maxima observed at these six airports. At Phoenix, there is very strong downward motion between 1 km and 4 km from roughly 9 LST to 21 LST, and strong upward motion at night, especially near the surface. At Denver, there is very strong upward motion at all height levels shown from 14 LST to 22 LST, weaker upward motion between 2 km and 4 km overnight, and downward motion between 2 km and 5 km from 9 LST to 12 LST.

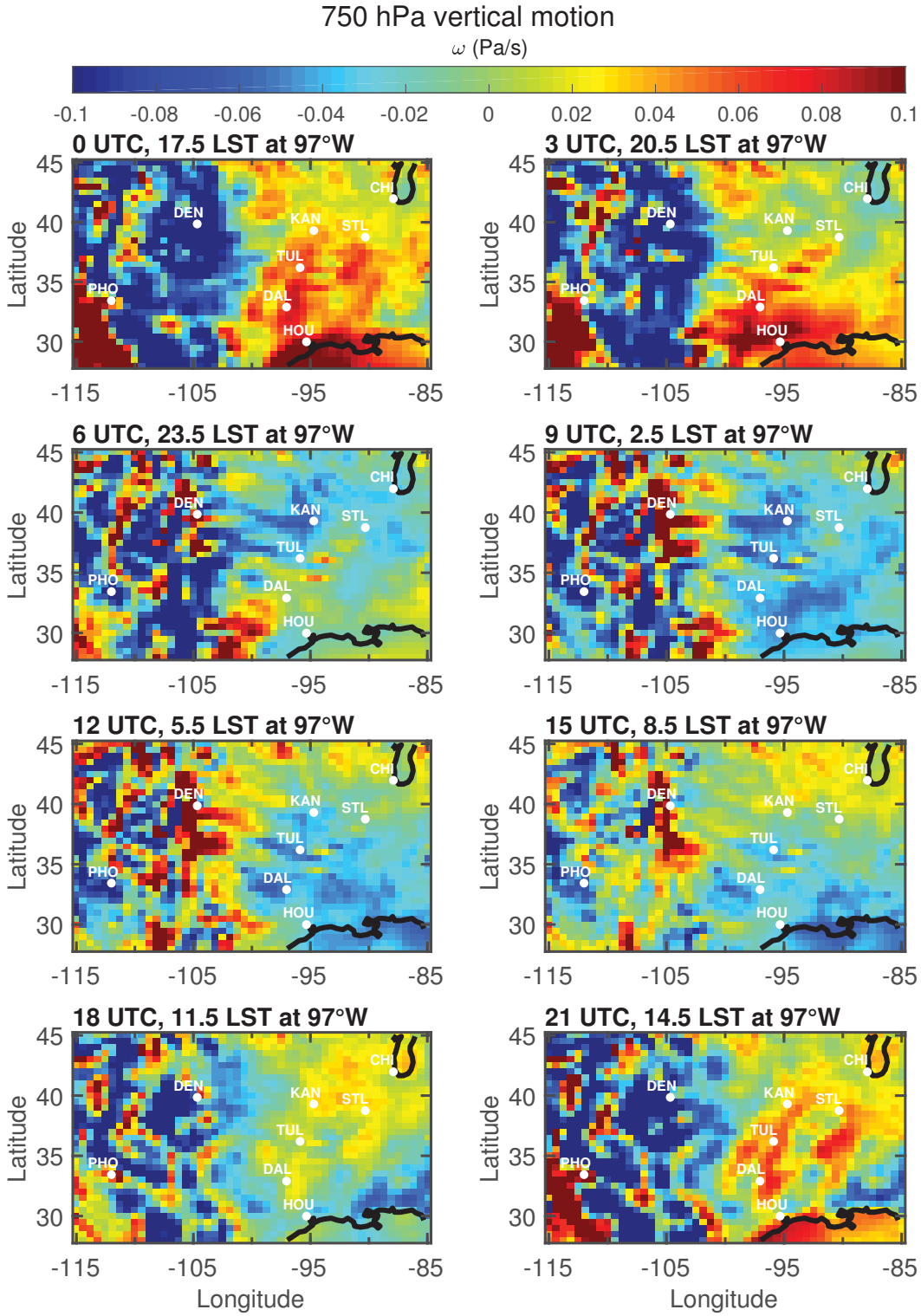

Figure 2.10: Spatial and diurnal variation of JJA 750 hPa vertical winds [Pa/s] from MERRA-2. Data from JJA of 2005 to 2014 are used in order to be consistent with the ACARS time period. Note the daytime downward motion and nocturnal upward motion at each of the six midwestern sites.

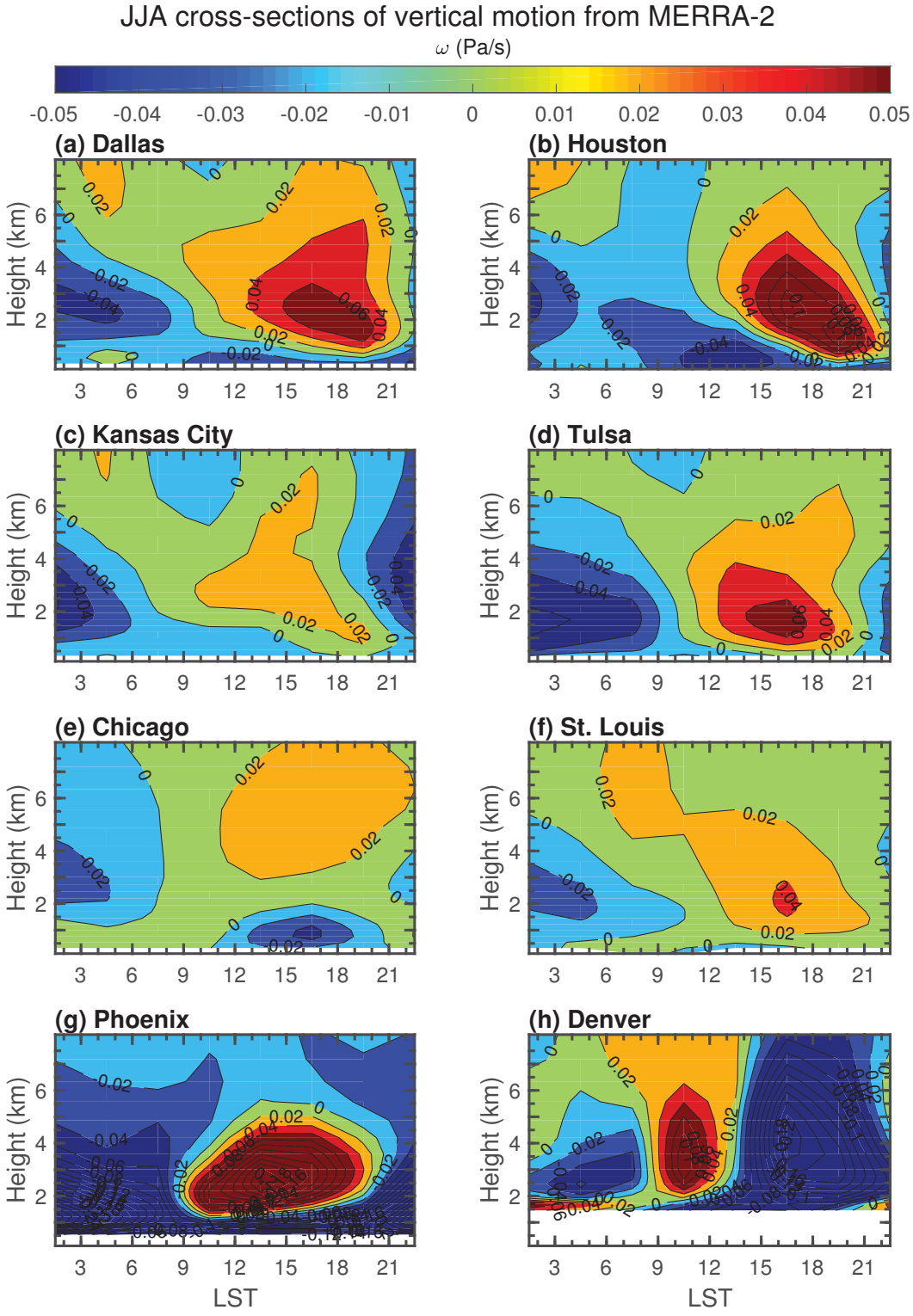

Figure 2.11: JJA cross-sections of vertical winds [Pa/s] at (a) Dallas, (b) Houston, (c) Kansas City, (d) Tulsa, (e) Chicago, (f) St. Louis, (g) Phoenix and (h) Denver from MERRA-2. Data are averaged over JJA of 2005 to 2014. At the six midwestern sites, there is upward motion between 2 km and 3 km overnight.

Figure 2.12 shows the diurnal cycle of 750 hPa vertical motion at Dallas during each season of 2011. The diurnal variation of vertical motion is weakest in winter (Nov.-Feb.), increases during spring (March-April), is strongest during summer (May-Aug.), and weakens in the fall (Sept.-Oct.).

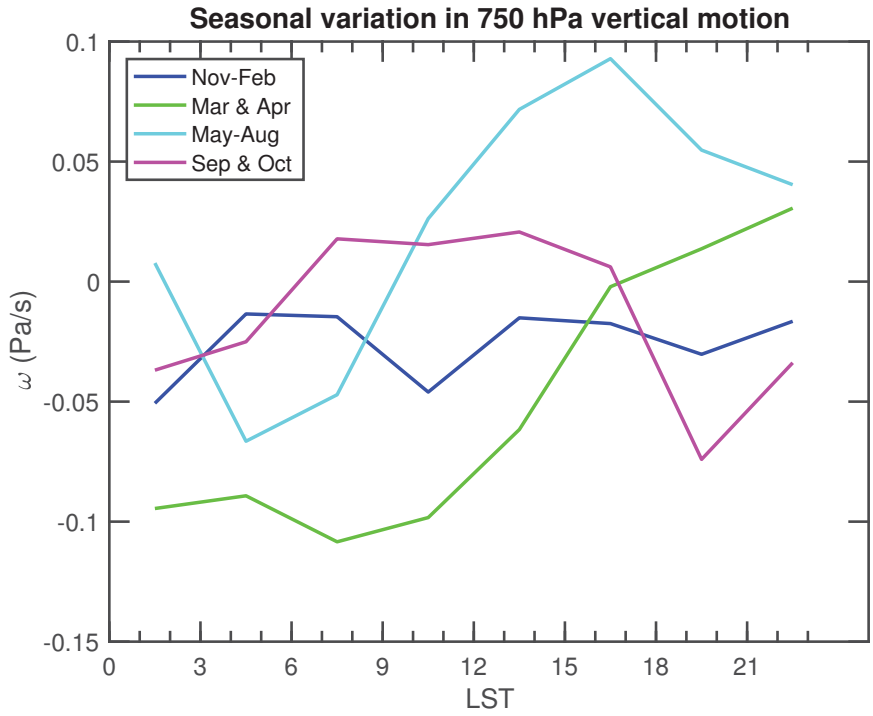

Figure 2.12: Seasonal variation in 750 hPa vertical motion [Pa/s] at Dallas during 2011. The largest diurnal variation in vertical motion occurs during the summer months (May-August).

Figure 2.13 shows diurnal cross-sections of MERRA-2 relative humidity during JJA 2011 at each of the eight airport locations. The overall diurnal variation of MERRA-2 relative humidity in the boundary layer is similar to that from ACARS (Fig.2.8). However, the observed very distinct 2011 2.5 km nocturnal relative humidity maxima are either not present, or, in the case of Dallas and Houston, much weaker than observed. At Denver, the near surface to 3 km relative humidity maximum between 3 LST and 9 LST shown in Fig. 2.8 is not captured by the reanalysis.

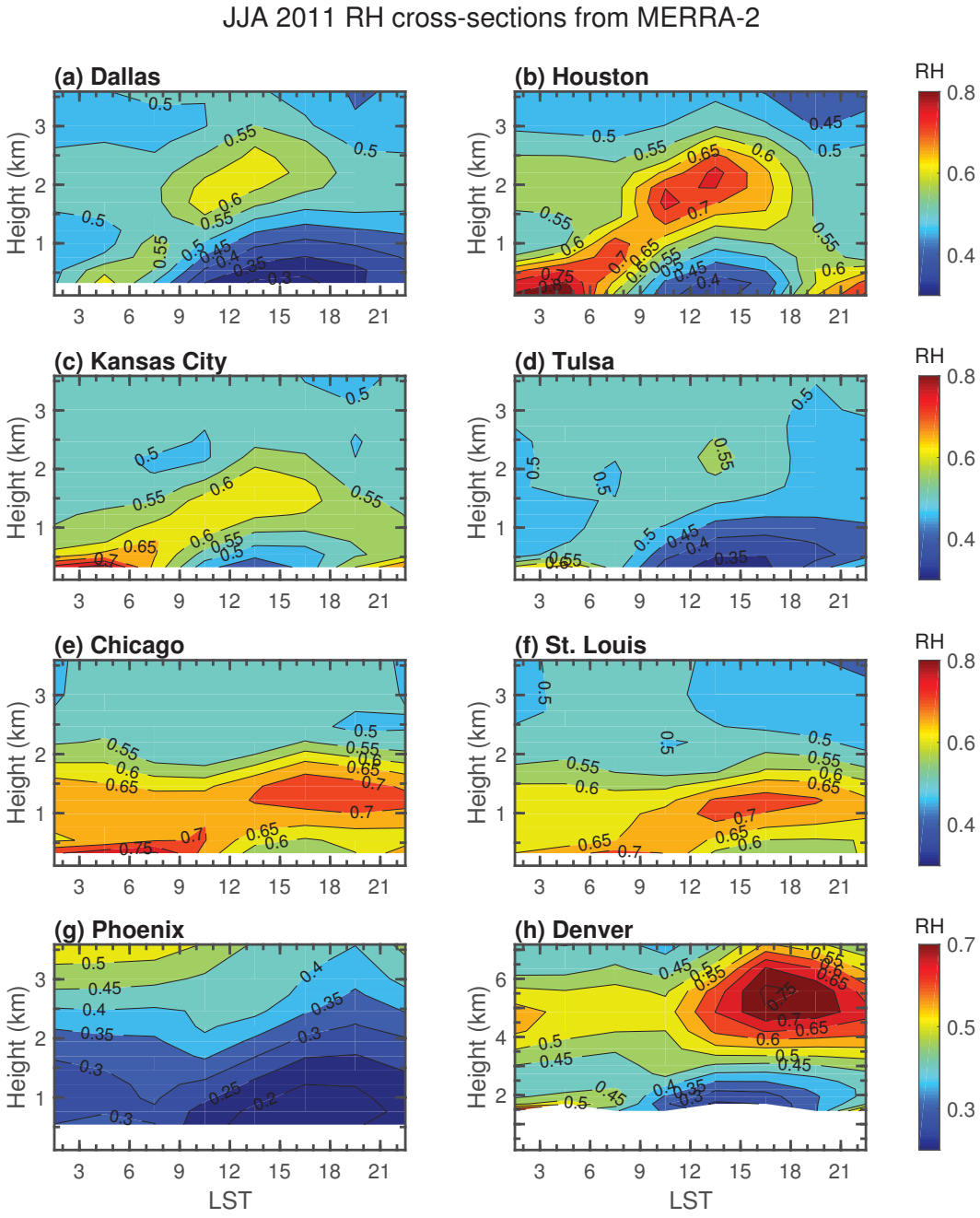

Figure 2.13: JJA cross-sections of MERRA-2 relative humidity at (a) Dallas, (b) Houston, (c) Kansas City, (d) Tulsa, (e) Chicago, (f) St. Louis, (g) Phoenix and (h) Denver during 2011. MERRA-2 underrepresents the nocturnal relative humidity maxima observed at 2.5 km in the Midwest.

Next, we investigate whether or not the diurnal variation in vertical wind of the MERRA-2 reanalysis is consistent with the amplitude of the observed diurnal variation in relative humidity between 2 km and 3 km in the Midwest. First, we obtained JJA diurnal q cross-sections at each airport from the MERRA-2 relative humidity and temperature JJA mean diurnal cross-sections over the ten year period (2005-2014). The temperature cross-sections were used to calculate the saturation vapour pressure. We then calculated the vapour pressure from the relative humidity and saturation vapour pressure. The diurnal q cross-sections were then calculated from the vapour pressure and pressure. If we ignore horizontal advection and source terms, and assuming the use of long term mean variables is appropriate, the local q tendency can be expressed as

$$\frac{\partial q}{\partial t} = -\omega \frac{\partial q}{\partial P} \tag{2.1}$$

This expression given in equation 2.1 was used to calculate the q tendency in units of per hour as a function of pressure and time of day, at each of the eight airports, using the local MERRA-2 JJA average values of ω and q. The local q tendency was then used to calculate the change in relative humidity in response to the MERRA-2 vertical motion, but in which the temperature was kept fixed at the JJA mean. The resulting relative humidity tendency is shown in the top panel of Figure 2.14. After midnight, there is a positive relative humidity tendency that is largest between 2 km and 3.5 km, and persists until roughly 8 LST. During the day, from roughly 12 LST to 21 LST, there is a negative relative humidity tendency between 2 km and 3.5 km.

Similarly, if horizontal advection and diabatic heating are ignored in the thermodynamic energy equation, and assuming the use of long term mean variables is appropriate, then the local rate of temperature change on a pressure surface can be expressed as

$$\frac{\partial T}{\partial t} = \omega \left[\frac{\Gamma_d - \Gamma}{\rho g} \right] \tag{2.2}$$

where Γ_d is the dry adiabatic lapse rate (9.8K/km), $\Gamma = -\frac{\Delta T}{\Delta z}$, and g is the acceleration due to gravity ($9.8 m/s^2$). The air density, ρ was calculated from the pressure and the temperature climatological cross-section. This temperature tendency was applied to the MERRA-2 climatological temperature cross-section. Figure 2.14 (b) shows the relative humidity tendency at Dallas associated with the diurnal changes

in temperature generated by vertical motion. The pattern is very similar to that in fig. 2.14 (a), but the magnitudes are weaker.

Figure 2.14 (c) shows the relative humidity tendency at Dallas associated with diurnal changes in vertical motion, and its effect on both q and temperature. The overall pattern is similar to the patterns from changes in q and temperature individually.

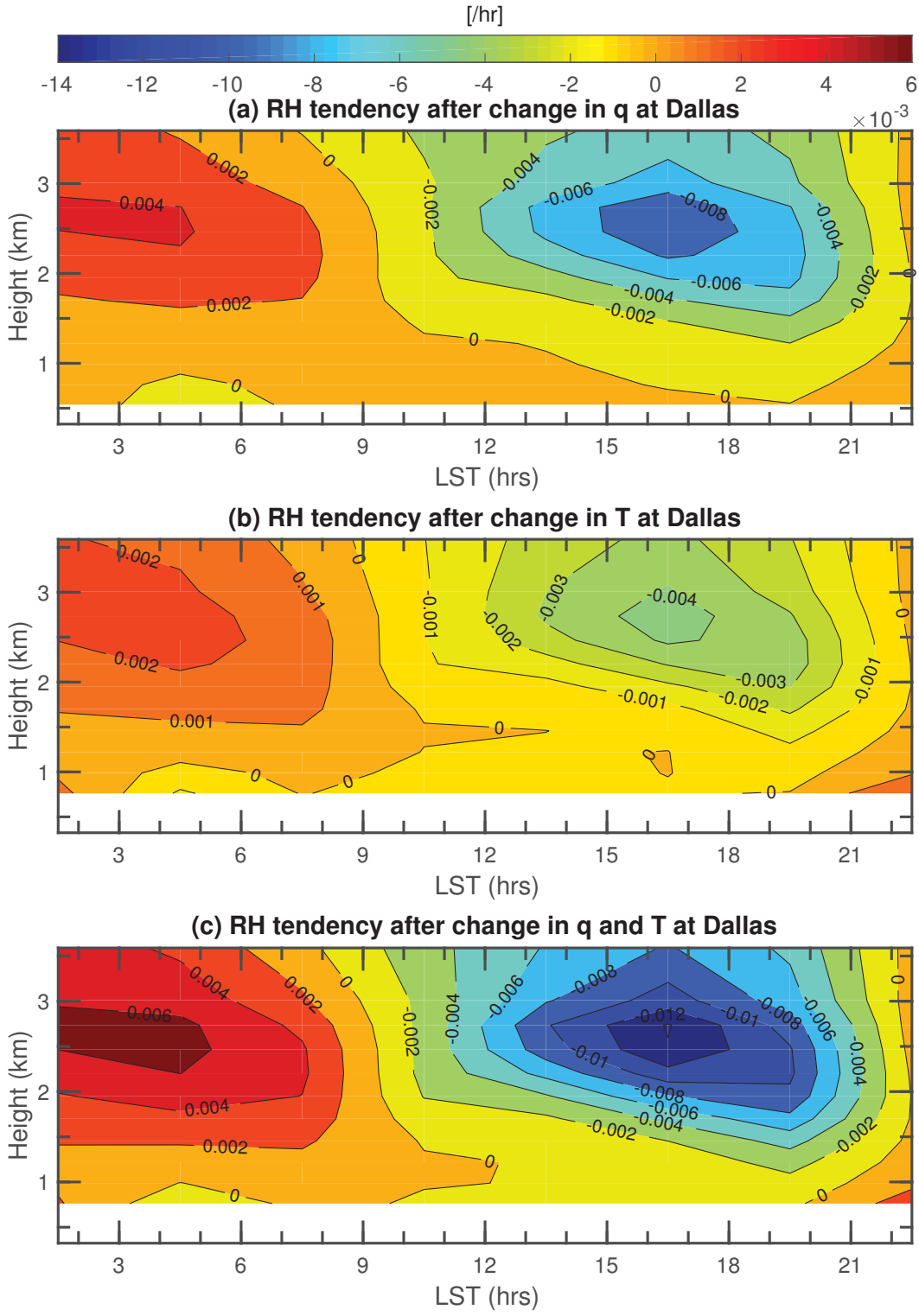

Figure 2.14: JJA cross-sections of MERRA-2 relative humidity tendency [/hr] at Dallas associated with vertical motion. Panel (a) shows the relative humidity tendency after changes in q generated by vertical motion. Panel (b) shows the relative humidity tendency after changes in temperature generated by vertical motion. Panel (c) shows the relative humidity tendency after changes in both q and temperature.

Next, we used the relative humidity tendency in each time-height bin to calculate the associated diurnal variation in relative humidity. We applied the relative humidity tendencies over a 24 hour period. Then we calculated the diurnal mean relative humidity at each height and subtracted it from the relative humidity in each time-height bin. The diurnal relative humidity anomaly generated by vertical motion is shown in Figure 2.15(a). Fig. 2.15(b) shows the observed relative humidity anomalies from ACARS for comparison. The relative humidity diurnal amplitude between 2 km and 3 km generated by the MERRA-2 vertical motion field is roughly equal in magnitude to that observed from the ACARS dataset. However, the diurnal variation in relative humidity generated by the MERRA-2 vertical motion field lags the observed diurnal variation in relative humidity by roughly three hours.

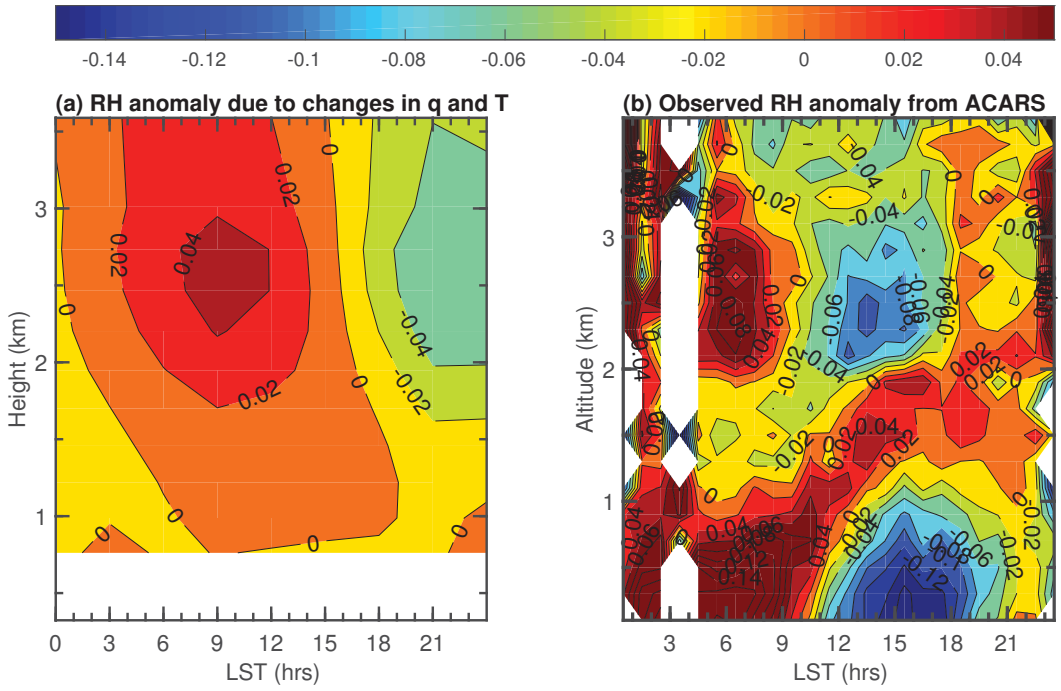

Figure 2.15: JJA diurnal cross-sections of (a) MERRA-2 relative humidity anomaly at Dallas, associated with diurnal changes in q and T generated by vertical motion, and (b) observed relative humidity anomaly from ACARS.

2.7 Nocturnal LLJ

The nocturnal LLJ is an important source of moisture for nocturnal convection over the Midwest (Stull 1988; Higgins et al. 1997; Berg et al. 2015). The LLJ is also associated with a strong diurnal variation in ageostrophic wind, which would be associated with a diurnal variation in vertical motion. The vertical circulations associated with the LLJ are likely to be coupled with the lower tropospheric mountain-plains solenoid, and could also be at least partially responsible for the observed nocturnal relative humidity anomalies near 2.5 km.

Fig. 2.16 shows a comparison of ACARS and MERRA-2 diurnal cycles of wind speed (a,b), zonal wind, u (c,d), and meridional wind, v (e,f), at Dallas. Winds are averaged over JJA 2005-2014. In the ACARS observations, the nocturnal LLJ first appears near 20 LST between 0.5 and 1.5 km and persists until 8 LST (Fig. 2.16(a)). The LLJ is mainly southerly with a weak zonal component that switches from easterly to westerly near midnight. The LLJ is quite well represented by the MERRA-2 reanalysis. For example, the analysis captures the zonal wind direction change near midnight, from easterly to westerly.

In the boundary layer during the day, there is an approximate three-way balance between the pressure gradient force, coriolis force and friction (Holton 2004). At sunset, the daytime CBL collapses, and frictional deceleration associated with turbulent momentum transport becomes restricted to a shallow surface layer. Above this layer, there is an imbalance between the pressure gradient force and the coriolis force. As a result, winds above the nocturnal boundary layer accelerate and become supergeostrophic (Blackadar 1957). The wind vector then rotates about the geostrophic wind vector in an inertial oscillation of period $\frac{2\pi}{f}$, where f is the coriolis parameter. Figure 2.17 shows a comparison of ACARS and MERRA-2 wind hodographs at Dallas during JJA 2005-2014. Unlike traditional hodographs, the points represent different times of day (LST). The colors represent different heights and are labelled in the plot legends.

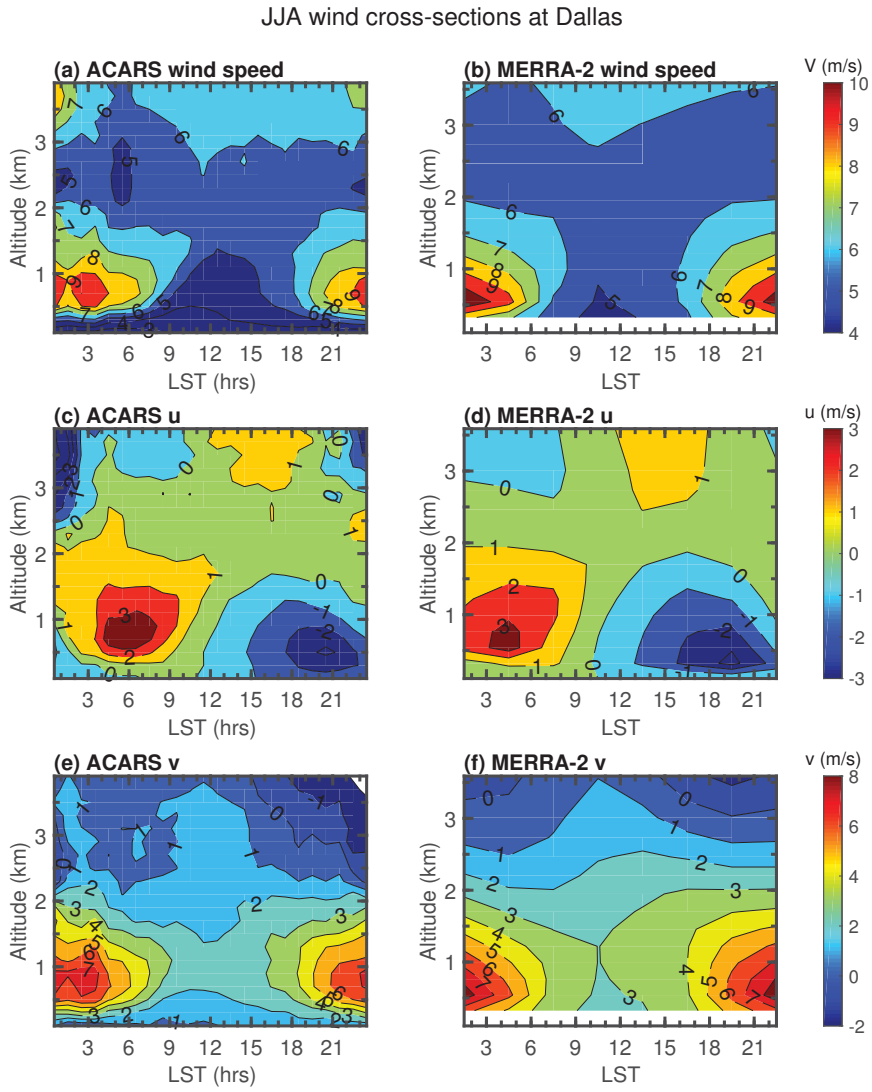

Figure 2.16: JJA mean diurnal cross-sections of wind speed (a,b), u (c,d) and v (e,f) in the Dallas area from ACARS and MERRA-2 [m/s]. Data from 2005 to 2014 are used. The nocturnal LLJ maximum spans between 500 m and 900 m. The zonal direction of the LLJ switches from easterly to westerly near midnight.

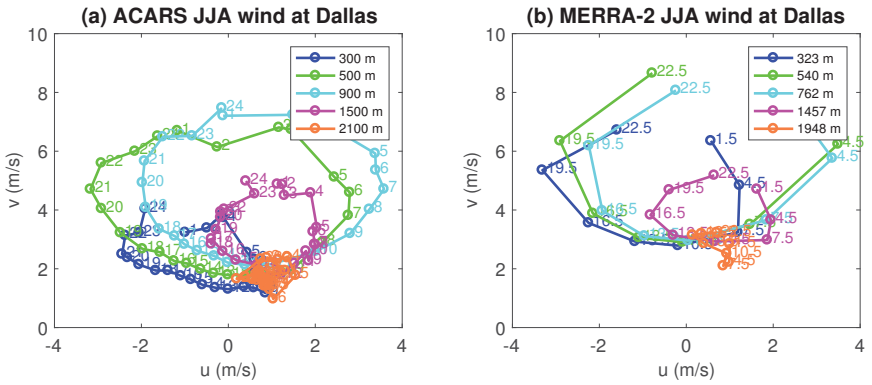

Figure 2.17: JJA hodographs [m/s] at Dallas from (a) ACARS and (b) MERRA-2. Here, points represent different local times and the colors represent different heights. Note the circular shape of each hodograph from both datasets. The larger the circle, the greater the diurnal variation of friction.

Both the ACARS and MERRA-2 hodographs have a circular shape. The size of the circles roughly represents the magnitude of the diurnal variation of friction at each height. The largest diurnal variation in friction occurs between 500 m and 900 m. Fig. 2.16(a) shows that the LLJ maximum lies between these heights. Below and above this height interval, the circles are much smaller. Near 2 km (above the daytime boundary layer), the diurnal variation of friction appears to approach zero.

2.8 Conclusion

We have used measurements from commercial aircraft to show that, during the summer, there are overnight maxima in relative humidity between 2 km and 3 km at six airports in the American Midwest. These relative humidity maxima are associated with negative anomalies in temperature and positive anomalies in specific humidity, as would be expected if they were generated by upward motion. We used MERRA-2 reanalysis data to show that, at each of these six airports, there is a diurnal variation in vertical motion in the lower troposphere with downward motion during the day and upward motion at night. The nocturnal relative humidity maxima therefore provide the strongest direct observational evidence to date of the existence of the mountain-plains solenoid, and offer a diagnostic for testing the strength of this diurnal circulation in climate models and reanalysis datasets. The magnitudes of the nocturnal relative humidity maxima appear to be underrepresented in the MERRA-2

reanalysis.

There is significant interannual variability in the magnitude of the summer nocturnal relative humidity maxima. This variability is coherent from year to year across each of the six midwestern airports. In 2011, for example, this feature was extremely strong, while in other years, such as 2014, it was almost non-existent. This is consistent with modelling studies which show that the mountain-plains solenoid is a delicate circulation whose strength can be modulated by the larger scale circulation or by surface properties such as soil moisture (Wolyn and McKee 1994).

Although the nocturnal relative humidity maxima are strongest during the summer months, they are present to some degree in the spring and fall. The strength of the mountain-plains solenoidal circulation should roughly scale with the strength of solar heating over the mountains. The seasonal variation of the relative humidity maxima is therefore also consistent with forcing by the mountain-plains solenoid.

The nocturnal LLJ is an important source of moisture to the American Midwest (Berg et al. 2015; Pitchford and London 1962; Higgins et al. 1997), and is associated with strong horizontal ageostrophic and vertical motions in the boundary layer. As such, it can also be expected to modulate the diurnal variation of relative humidity in the boundary layer, and to some extent, the diurnal variation of relative humidity in the lower free troposphere as well. However, because the diurnal variability in horizontal wind associated with the LLJ is restricted to below 2 km, it is not likely to be the main source of diurnal variability in relative humidity between 2 km and 3 km.

We also examined the diurnal variation in lower tropospheric relative humidity at Phoenix and Denver. These two locations are much closer to strong sources of orographic solar heating. As a result, the diurnal variation in lower tropospheric vertical motion at these two locations can be expected to be much stronger than at the six midwestern locations. At Phoenix, there is a strong positive anomaly in relative humidity at night between 2 km and 3 km. At Denver, there is a strong positive relative humidity anomaly starting in the afternoon. These diurnal variations in relative humidity are consistent with the strong diurnal variation in vertical motion at these two locations in the MERRA-2 reanalysis.

2.9 Acknowledgments

This study was supported by grants from NSERC [Natural Sciences and Engineering Research Council of Canada] and MEOPAR [Marine Environmental Observation Prediction and Response Network]. We thank Glen Lesins, Jeff Geddes, and Brian Boys for their useful suggestions.

Chapter 3

Conclusion and Future Work

We used commercial aircraft measurements from the ACARS dataset to construct summer mean diurnal vertical cross-sections of lower tropospheric relative humidity at six midwestern, and two mountain airports. At the six midwestern airports, the diurnal cross-sections of relative humidity had broadly similar patterns. Near the surface, there was an overnight maximum and a daytime minimum in relative humidity. During the daytime, the height of maximum boundary layer relative humidity reached a peak of 1.5 km to 2 km during the afternoon near 15 LST. These six cross-sections also showed an overnight relative humidity maximum between 2 km and 3 km from roughly 3 LST to 9 LST.

The relative humidity cross-sections at the two mountain airports were quite different. At Phoenix, the boundary layer was very dry, with a daytime surface minimum in relative humidity. Between 2 km and 3 km in altitude, a relative humidity maximum was observed both after sunset and during the early morning hours. At Denver, there was a daytime surface minimum in relative humidity. Above that, there was a maximum in relative humidity between 3 km and 6 km from late afternoon into the overnight hours.

The main purpose of the project was to investigate the existence and origin of the observed overnight relative humidity maxima above the boundary layer at the six midwestern sites. Using temperature and dew point measurements from the ACARS dataset, we constructed summer mean diurnal vertical cross-sections of temperature anomaly and fractional anomaly of specific humidity. We found that the relative humidity maxima coincide with both a negative anomaly in temperature and a positive anomaly in specific humidity.

There is significant interannual variability in the strength of the summer overnight relative humidity maxima. During the summer of 2011, the maxima were particularly strong at all six midwestern sites. However, during some years, such as 2014, the

maxima were not present at either of the midwestern sites. The coherent interannual variability of the relative humidity maxima across the midwestern sites, in combination with the associated anomalies in temperature and specific humidity, suggest that the relative humidity maxima are forced by nocturnal upward motion associated with a large scale circulation.

We used 750 hPa vertical winds from the MERRA-2 reanalysis to show that at each of the midwestern airports, there is downward motion during the daytime and upward motion overnight. This diurnal cycle of vertical motion east of the Rocky Mountains has been shown using other reanalysis datasets and has been attributed to the mountain-plains solenoidal circulation (Carbone and Tuttle 2008; Tuttle and Davis 2013). This circulation is known to be strongest during the summer months (Wolyn and McKee 1994). We found that the strength of the nocturnal relative humidity maxima is also strongest during the summer months, hence supporting the idea that the relative humidity maxima are a response to the strength of the mountain-plains solenoid.

We also used the MERRA-2 reanalysis dataset to plot diurnal vertical cross-sections of relative humidity at each of the chosen airports during the summer of 2011. This was the summer showing the strongest nocturnal relative humidity maxima above the boundary layer. However, the reanalysis very weakly represents overnight relative humidity maxima at 2.5 km if they are present in the reanalysis at all.

We then derived the relative humidity tendency associated with the vertical winds from the MERRA-2 dataset (over JJA 2005-2014). We found that the vertical motion field represented in the reanalysis could generate a diurnal amplitude in relative humidity between 2 km and 3 km that is comparable in magnitude to that observed by ACARS. It is not clear why the relative humidity maxima are underrepresented by the reanalysis, particularly since MERRA-2 assimilates the ACARS dataset (Gelaro et al. 2017).

The nocturnal LLJ was also studied in relation to the nocturnal relative humidity maxima, as it is a known moisture source to the Midwest. We found that the maximum southerly winds in the jet are constrained below 2 km. Hence, the LLJ is likely not the main contributor to the overnight relative humidity anomalies between 2 km

and 3 km. A comparison of the diurnal and vertical variation of the lower tropospheric horizontal winds from the MERRA-2 reanalysis with the ACARS observations, shows that the winds are represented well by the reanalysis. Wind hodographs from both ACARS and MERRA-2 show that there is an inertial oscillation in the boundary layer winds over the diurnal cycle.

Overall, the diurnal vertical cross-sections of lower tropospheric relative humidity may be used as a diagnostic for the existence and strength of the mountain-plains solenoid. The strength of both the relative humidity and the circulation roughly scale with the amount of solar heating. Also, the strength of the solenoidal circulation is known to depend on the strength of the ambient westerlies, boundary layer stability, and surface properties such as soil moisture (Wolyn and McKee 1994). The interannual variability in the strength of the relative humidity maxima is likely a response to changes in these properties and possibly others.

Future work should include developing a relationship between the strength of the mountain-plains solenoid and nocturnal convective rainfall over the American Midwest. The nocturnal peak in rainfall has been of great interest in the literature (Carbone and Tuttle 2008; Tuttle and Davis 2013; Li and Smith 2010). To do this, it would be best to look at observations over shorter timescales, rather than climatologies. The strength of the solenoidal circulation could be calculated as the relative strength of the nocturnal relative humidity maxima above the boundary layer. The strength of the relative humidity maxima could be evaluated in two ways: (i) as the difference between the maximum overnight relative humidity and the minimum daytime relative humidity within the 2-3 km layer or (ii) as the overnight vertical gradient in relative humidity between 1-2 km and 2-3 km.

References

A.Karipot, M. Leclerc, and G. Zhang, 2009: Characteristics of Nocturnal Low-Level Jets Observed in the North Florida Area. *Mon. Wea. Rev.*, **137**, 2605–2621, doi: 10.1175/2009MWR2705.1.

Baas, P., F. Bosveld, and H. K. Baltink, 2009: A Climatology of Nocturnal Low-Level Jets at Cabauw. *J. Appl. Meteor. Climatol.*, **48**, 1627–1642, doi:10.1175/ 2009JAMC1965.1.

Balling, R., 1985: Warm Season Nocturnal Precipitation in the Great Plains of the United States. *J. Climate Appl. Meteor.*, **24**, 1383–1387, doi:10.1175/ 1520-0450(1985)024⟨1383:WSNPIT⟩2.0.CO;2.

Banta, R., 1984: Daytime Boundary-Layer Evolution over Mountainous Terrain. Part 1: Observations of the Dry Circulations. *Mon. Wea. Rev.*, **112**, 340–356, doi:10. 1175/1520-0493(1984)112⟨0340:DBLEOM⟩2.0.CO;2.

Benjamin, S., B. Schwartz, and R. Cole, 1999: Accuracy of ACARS Wind and Temperature Observations Determined by Collocation. *Wea. Forecasting*, **14**, 1032–1038, doi:10.1175/1520-0434(1999)014⟨1032:AOAWAT⟩2.0.CO;2.

Berg, L., L. Riihimaki, Y. Qian, H. Yan, and M. Huang, 2015: The Low-Level Jet over the Southern Great Plains Determined from Observations and Reanalyses and Its Impact on Moisture Transport. *J. Climate*, **28**, 6682–6706, doi:10.1175/ JCLI-D-14-00719.1.

Blackadar, A., 1957: Boundary Layer Wind Maxima and Their Significance for the Growth of Nocturnal Inversions. *Bull. Amer. Meteor. Soc.*, **38**, 283–290.

Bonner, W., 1968: Climatology of the Low Level Jet. *Mon. Wea. Rev.*, **96**, 833–850.

Bossert, J., J. Sheaffer, and E. Reiter, 1989: Aspects of Regional-Scale Flows in Mountainous Terrain. *J. Appl. Meteor.*, **28**, 590–601, doi:10.1175/1520-0450(1989) 028⟨0590:AORSFI⟩2.0.CO;2.

Carbone, R., and J. Tuttle, 2008: Rainfall Occurrence in the U.S. Warm Season: The Diurnal Cycle. *J. Climate*, **21**, 4132–4146, doi:10.1175/2008JCLI2275.1.

Chan, K., and R. Wood, 2013: The seasonal cycle of planetary boundary layer depth determined using COSMIC radio occultation data. *J. Geophys. Res.*, **118**, 12,422–12,434, doi:10.1002/2013JD020147.

Cheng-Ying, D., G. Zhi-Qiu, Q. Qing, and C. Gang, 2011: Analysis of Atmospheric Boundary Layer Height Characteristics over the Arctic Ocean Using the Aircraft and GPS Soundings. *Atmos. Oceanic Sci. Lett.*, **4**, 124–130.

Dai, A., 2006: Recent Climatology, Variability, and Trends in Global Surface Humidity. *J. Climate*, **19**, 3589–3606, doi:10.1175/JCLI3816.1.

Dai, A., and J. Wang, 1999: Diurnal and Semidiurnal Tides in Global Surface Pressure Fields. *J. Atmos. Sci.*, **56**, 3874–3891, doi:10.1175/1520-0469(1999)056⟨3874:DASTIG⟩2.0.CO;2.

Ek, M., and L. Mahrt, 1994: Daytime Evolution of Relative Humidity at the Boundary Layer Top. *Mon. Wea. Rev.*, **122**, 2709–2721, doi:10.1175/1520-0493(1994)122⟨2709:DEORHA⟩2.0.CO;2.

Ferrare, R., and Coauthors, 2003: Lidar characterizations of water vapor measurements over the ARM SGP site. *Symposium on observing and understanding the variability of water and climate*, Long Beach, CA, Amer. Meteor. Soc., JP2.9, [Available online at https://ams.confex.com/ams/annual2003/techprogram/paper_56233.htm.].

Garratt, J., 1992: *The atmospheric boundary layer*. Cambridge University Press, 316 pp.

Geerts, B., and Coauthors, 2016: The 2015 Plains Elevated Convection At Night (PECAN) field project. *Bull. Amer. Soc.*, **98**, 767–786, doi:10.1175/BAMS-D-15-00257.1.

Gelaro, R., and Coauthors, 2017: The Modern-Era Retrospective Analysis for Research and Applications, Version 2 (MERRA-2). *J. Cli.*, **in press**, doi:10.1175/JCLI-D-16-0758.1.

GMAO, 2015: MERRA-2 inst3_3d_asm_Np: 3d, 3-Hourly, Instantaneous, Pressure-Level Assimilation, Assimilated Meteorological Fields, Version 5.12.4. *Goddard Space Flight Center Distributed Active Archive Center (GSFC DAAC)*, doi:10.5067/QBZ6MG944HW0.

Guo, P., K. Y.-H, S. Sokolovskiy, and D. Lenschow, 2011: Estimating Atmospheric Boundary Layer Depth Using COSMIC Radio Occultation Data. *J. Atmos. Sci.*, **68**, 1703–1713, doi:10.1175/2011JAS3612.1.

Higgins, R., Y. Yao, E. Yarosh, J. Janowiak, and K. Mo, 1997: Influence of the Great Plains Low-Level Jet on Summertime Precipitation and Moisture Transport over the Central United States. *J. Climate*, **10**, 481–507, doi:10.1175/2009JAS3247.1.

Holton, J., 2004: *An Introduction to Dynamic Meteorlogy*. Elsevier Academic Press, 535 pp.

Jiang, X., N.-C. Lau, and S. Klein, 2006: Role of eastward propagating convection systems in the diurnal cycle and seasonal mean of summertime rainfall over the U.S. Great Plains. *Geophys. Res. Lett.*, **33**, L19 809, doi:10.1029/2006GL027022.

Klein, P., X.-M. Hu, A. Shapiro, and M. Xue, 2015: Linkages Between Boundary-Layer Structure and the Development of Nocturnal Low-Level Jets in Central Oklahoma. *Boundary-Layer Meteorology*, **158**, 383–408, doi:10.1007/s10546-015-0097-6.

Li, Y., and R. Smith, 2010: The Detection and Significance of Diurnal pressure and Potential Vorticity Anomalies East of the Rockies. *J. Atmos. Sci.*, **67**, 2734–2751, doi:10.1175/2010JAS3423.1.

Lindzen, R., and S. Chapman, 1970: *Atmospheric Tides*. D. Reidel, 200 pp.

Liu, S., and X.-Z. Liang, 2010: Observed Diurnal Cycle Climatology of Planetary Boundary Layer height. *J. Climate*, **23**, 5790–5809, doi:10.1175/2010JCLI3552.1.

Mamrosh, R., R. Baker, and T. Jirikowic, 2002: A comparison of ACARS WVSS and NWS radiosonde temperature and moisture data. *Sixth Symposium on Integrated Observing Systems*, Orlando, FL, Amer. Meteor. Soc., 6.1.4, [Available online at https://ams.confex.com/ams/pdfpapers/30088.pdf.].

McCarty, W., L. Coy, R. Gelaro, A. Huang, D. Merkova, E. Smith, M. Sienkiewicz, and K. Wargan, 2016: MERRA-2 Input Observations: Summary and Assessment. *NASA Tech. Rep. NASA/TM-2016-104606*, **46**, 51, [Available online at https://gmao.gsfc.nasa.gov/pubs/docs/McCarty885.pdf.].

McGrath-Spangler, E., and A. Denning, 2013: Estimating climatological planetary boundary layer heights from radiosonde observations: Comparisons of methods and uncertainty analysis. *J. Geophys. Res.*, **118**, 1226–1233, doi:10.1002/jgrd.50198.

Monaghan, A., D. Rife, J. Pinto, and C. Davis, 2010: Global Precipitation Extremes Associated with Diurnally Varying Low-Level Jets. *J. Climate*, **23**, 5065–5084, doi:10.1175/2010JCLI3515.1.

Moninger, W., R. Mamrosh, and P. Pauley, 2003: Automated Meteorological Reports From Commercial Aircraft. *Bull. Amer. Meteor. Soc.*, **28**, 203–216, doi:10.1175/BAMS-84-2-203.

Nicholson, S., 2016: The Turkana low-level jet: mean climatology and association with regional aridity. *Int. J. Climatol.*, **36**, 2598–2614, doi:10.1002/joc.4515.

Pitchford, K., and J. London, 1962: The Low-Level Jet as Related to Nocturnal Thunderstorms over Midwest United States. *J. Appl. Meteor.*, **1**, 43–47, doi:10.1175/1520-0450(1962)001,0043:TLLJAR.2.0.CO;2.

Pu, B., and R. Dickinson, 2014: Diurnal Spatial Variability of Great Plains Summer Precipitation Related to the Dynamics of the Low-Level Jet. *J. Atmos. Sci.*, **71**, 1807–1817, doi:10.1175/JAS-D-13-0243.1.

Reif, D., and H. Bluestein, 2017: A 20-Year Climatology of Nocturnal Convection Initiation over the Central and Southern Great Plains during the Warm Season. *Mon. Wea. Rev.*, **145**, 1615–1639, doi:10.1175/MWR-D-16-0340.1.

Ruzmaikin, A., H. Aumann, and E. Manning, 2014: Relative Humidity in the Troposphere with AIRS. *J. Atmos. Sci.*, **71**, 2516–2533, doi:10.1175/JAS-D-13-0363.1.

Schmid, P., and D. Niyogi, 2012: A Method for Estimating Planetary Boundary Layer Heights and Its Application over the ARM Southern Great Plains Site. *J. Atmos. Oceanic Technol.*, **29**, 316–322, doi:10.1175/JTECH-D-11-00118.1.

Schwartz, B., and S. Benjamin, 1995: A Comparison of Temperature and Wind Measurements from ACARS-Equipped Aircraft and Rawinsondes. *Wea. Forecasting*, **10**, 528–544, doi:10.1175/1520-0434(1995)010⟨0528:ACOTAW⟩2.0.CO;2.

Seidel, D., C. Ao, and K. Li, 2010: Global seasonal variations of midday planetary boundary layer depth from CALIPSO space-borne LIDAR. *J. Geophys. Res.*, **115**, D16 113, doi:10.1029/2009JD013680.

Sjostedt, D., J. Sigmon, and S. Colucci, 1990: The Carolina Nocturnal Low-Level Jet: Synoptic Climatology and a Case Study. *Wea. Forecasting*, **5**, 404–415, doi:10.1175/1520-0434(1990)005⟨0404:TCNLLJ⟩2.0.CO;2.

Song, J., K. Liao, R. Coulter, and B. Lesht, 2005: Climatology of the Low-Level Jet at the Southern Great Plains Atmospheric Boundary Layer Experiments Site. *J. Appl. Meteor.*, **44**, 1593–1606, doi:10.1175/JAM2294.1.

Stull, R., 1988: *An Introduction to Boundary Layer Meteorlogy*. Kluwer Academic, 666 pp.

Sullivan, J., and Coauthors, 2016: Quantifying the contribution of thermally driven recirculation to a high ozone event along the Colorado Front Range using lidar. *J. Geophys. Res.*, **121**, 10,377–10,390, doi:10.1002/2016JD025229.

Teixeira, J., 2001: Cloud Fraction and Relative Humidity in a Prognostic Cloud Fraction Scheme. *Mon. Wea. Rev.*, **129**, 1750–1753, doi:10.1175/1520-0493(2001)129⟨1750:CFARHI⟩2.0.CO;2.

Trier, S., C. Davis, and D. Ahijevych, 2010: Environmental Controls on the Simulated Diurnal Cycle of Warm-Season Precipitation in the Continental United States. *J. Atmos. Sci.*, **67**, 1066–1090, doi:10.1175/1520-0442(1997)010⟨0481:IOTGPL⟩2.0.CO;2.

Tripoli, G., and W. Cotton, 1989: Numerical Study of an Observed Orogenic Mesoscale Convective System. Part 1: Simulated Genesis and Comparison with Observations. *Mon. Wea. Rev.*, **117**, 273–304, doi:10.1175/1520-0493(1989)117⟨0273:NSOAOO⟩2.0.CO;2.

Tuttle, J., and C. Davis, 2006: Corridors of Warm Season Precipitation in the Central United States. *Mon. Wea. Rev.*, **134**, 2297–2317, doi:10.1175/MWR3188.1.

Tuttle, J., and C. Davis, 2013: Modulation of the Diurnal Cycle of Warm-Season Precipitation by Short-Wave Troughs. *J. Atmos. Sci.*, **70**, 1710–1726, doi:10.1175/JAS-D-12-0181.1.

von Elgin, A., and J. Teixeira, 2013: A Planetary Boundary Layer Height Climatology derived from ECMWF Re-analysis Data. *J. Climate*, **26**, 6575–6590, doi:10.1175/JCLI-D-12-00385.1.

Wolyn, P., and T. McKee, 1994: The Mountain-Plains Circulation East of a 2-km-High North-South Barrier. *Mon. Wea. Rev.*, **122**, 1490–1508, doi:10.1175/1520-0493(1994)122⟨1490:TMPCEO⟩2.0.CO;2.

Wu, Y., and S. Raman, 1998: The Summertime Great Plains Low Level Jet and the Effect of its Origin on Moisture Transport. *Boundary-Layer Meteorology*, **88**, 445–466, doi:10.1023/A:1001518302649.

Zhang, Y., and S. Klein, 2013: Factors Controlling the Vertical Extent of Fair-Weather Shallow Cumulus Clouds over Land: Investigation of Diurnal-Cycle Observations Collected at the ARM Southern Great Plains Site. *J. Atmos. Sci.*, **70**, 1297–1315, doi:10.1175/JAS-D-12-0131.1.

Zhang, Y., F. Zhang, and J. Sun, 2014: Comparison of the diurnal variations of warm-season precipitation for East Asia vs. North America downstream of the Tibetan Plateau vs. the Rocky Mountains. *Atmos. Chem. Phys.*, **14**, 10,741–10,759, doi:10.5194/acp-14-10741-2014.

Zipser, E., 1969: The Role of Organized Unsaturated Convective Downdrafts in the Structure and Rapid Decay of an Equatorial Disturbance. *J. Appl. Meteor.*, **8**, 799–814, doi:10.1175/1520-0450(1969)008⟨0799:TROOUC⟩2.0.CO;2.

APPENDIX A

A.1 Copyright Information

Chapter 2 of this thesis contains an article that has been submitted for publication, and is currently in revision. Copyright in this work may be transferred without further notice, and this version may no longer be accessible.